AAPS PharmSciTech (2022) 23: 127
https://doi.org/10.1208/s12249-022-02270-4

RESEARCH ARTICLE

Evaluation of Piperine as Natural Coformer for Eutectics Preparation of Drugs Used in the Treatment of Cardiovascular Diseases

Krissia Wilhelm-Romero[1,2] · María Isabel Quirós-Fallas[2] · José Roberto Vega-Baudrit[1,3] · Teodolito Guillén-Girón[4] · Felipe Vargas-Huertas[2] · Mirtha Navarro-Hoyos[2] · Andrea Mariela Araya-Sibaja[1,5]

Received: 10 January 2022 / Accepted: 3 April 2022 / Published online: 26 April 2022

Abstract

Piperine (PIP) was evaluated as a natural coformer in the preparation of multicomponent organic materials for enhancing solubility and dissolution rate of the poorly water-soluble drugs: curcumin (CUR), lovastatin (LOV), and irbesartan (IBS). A screening based on liquid assisted grinding technique was performed using 1:1 drug-PIP molar ratio mixtures, followed by differential scanning calorimetry (DSC) and powder X-ray diffraction (PXRD) analyses. Three eutectic mixtures (EMs) composed of CUR-PIP, LOV-PIP, and IBS-PIP were obtained. Therefore, binary phase and Tamman's diagrams were constructed for each system to obtain the exact eutectic composition, which was 0.41:0.59, 0.29:0.71, and 0.31:0.69 for CUR-PIP, LOV-PIP, and IBS-PIP, respectively. Further, bulk materials of each system were prepared to characterize them through DSC, PXRD fully, Fourier transform infrared spectroscopy (FT-IR), and solution-state nuclear magnetic resonance (NMR) spectroscopy. In addition, the contact angle, solubility, and dissolution rate of each system were evaluated. The preserved characteristic in the PXRD patterns and FT-IR spectra of the bulk material of each system confirmed the formation of EM mixture without molecular interaction in solid-state. The formation of EM resulted in improved aqueous solubility and dissolution rate associated with the increased wettability observed by the decrease in contact angle. In addition, solution NMR analyses of CUR-PIP, LOV-PIP, and IBS-PIP suggested no significant intermolecular interactions in solution between the components of the EM. Hence, this study concludes that PIP could be an effective coformer to improve the solubility and dissolution rate of CUR, LOV, and IBS.

KEY WORDS curcumin · eutectics · irbesartan · lovastatin · multicomponent organic materials · piperine · solid-state characterization

INTRODUCTION

According to the WHO, approximately 17.9 million lives have been lost due to cardiovascular disease (CVD) only during 2019 (1). People at risk of developing CVD can show uncontrolled increases in blood pressure, high levels of glucose, and lipids, which are potentiated with secondary diseases such as obesity, being overweight, and increasing cholesterol (1). Further, CVD represents high medical costs for the population and governments (2, 3). In Costa Rica, it is estimated that CVD costs the healthcare system nearly $ 422 million annually in inpatient care, including hospitalizations, outpatient consultations, and attention in the emergency service (4). Ideally, the best strategies to reduce mortality from CVD are prevention policies to decrease trends in risk factors (5). However, although efforts were made in that direction, significant gaps persist to control

✉ Andrea Mariela Araya-Sibaja
aaraya@cenat.ac.cr

1 Laboratorio Nacional de Nanotecnología LANOTEC-CeNAT-CONARE, 1174-1200 Pavas, San José, Costa Rica

2 Escuela de Química, Laboratorio BIODESS, Universidad de Costa Rica, San Pedro de Montes de Oca 2060, San José, Costa Rica

3 Laboratorio de Investigación y Tecnología de Polímeros POLIUNA, Escuela de Química, Universidad Nacional de Costa Rica, Heredia 86-3000, Costa Rica

4 Centro de Investigación y Extensión en Materiales, Escuela de Ciencia E Ingeniería de los Materiales, Tecnológico de Costa Rica, Cartago 159-7050, Costa Rica

5 Universidad Técnica Nacional, Alajuela 159-7050, Costa Rica

cardiovascular diseases, especially in the elderly population that presents greater probabilities for the development of CVDs (6). Therefore, it is essential to find, along with traditional medicine, new alternatives to reduce complications and slow the progression of CVD (7).

Lovastatin (LOV) and irbesartan (IBS) are commercial drugs used to treat CVD as antihyperlipidemic and antihypertensive, respectively. In addition, LOV has been reported as a prophylactic agent in managing morbidities, including peripheral arterial disease, atherosclerosis, sepsis, cerebrovascular disease, ischemic disease, and bone fracture (8). While IBS has been found to be effective in the treatment of hypertension-related cardiovascular end-organ damage (9). On the other hand, studies on the natural polyphenol curcumin (CUR) have demonstrated highly beneficial cardio-protective properties, diminishing myocardial ischemia/reperfusion injury, cardiac hypertrophy, drug-induced cardiotoxicity, arrhythmia, hypertrophic cardiomyopathy, heart failure, atherosclerosis, aortic aneurysm, stroke, and diabetic cardiovascular complications. These effects are mainly attributed to its anti-inflammatory, oxidative stress decrease, and apoptosis mechanisms (10, 11); therefore, representing an attractive natural alternative in CVD treatment.

The beneficial effects of LOV, IBS, and CUR are however constraint mainly because of their poor water solubility limiting their bioavailability. In addition, the bioavailability of these molecules is also affected by the glucuronidation pathway (12–15), which is the primary metabolic pathway of xenobiotics in mammalian species (16). This mechanism is usually observed in class II and IV drugs in the Biopharmaceutical Classification System (17). In this regard, piperine (PIP) has been reported to exhibit inhibition of the glucuronidation pathway (12–15). Hence, the interest is to study PIP in conjunction with class II and IV molecules to improve their bioavailability associated with the glucuronidation mechanism.

In terms of increasing solubility, multicomponent organic material (MOM) preparation is a powerful approach to improving class II and IV drugs (18). Eutectic mixtures (EMs) are MOM types that possess characteristics that increase solubility, such as lower melting point than pure compounds, reduced particle size, and lower process temperatures (19). EMs are prepared using the target molecule that needs solubility improvement along with a second molecule acting as a coformer. The coformers are selected according to their electrostatic and non-covalent interactions and can be both non-active or active molecules having a synergic or complementary therapeutic effect (20). For instance, drugs have been used as coformers for EM formation in multi-drug therapy (21–23).

In this context, PIP has been reported as CUR's bioenhancer able to increase the solubility and bioavailability, preventing its early excretion. The mechanism has been proposed by Singh *et al*. (1986) and Wang *et al*. (2019) (24, 25) and is presented in Fig. 1 for illustration. In addition, PIP is reported to have low toxicity in either animals or humans, even at high doses, and it is classified as generally regarded as a safe (GRAS) substance (26).

This study focuses on the preparation of EM from CUR, LOV, and IBS using PIP as a coformer to improve the solubility, dissolution rate, and consequently the bioactivities of these poorly water-soluble molecules. The chemical structure of PIP, CUR, LOV, and IBS are presented in Fig. 2. Differential scanning calorimetry (DSC) data were used to construct binary phase and Tammann's diagrams. Bulk materials of the three eutectic systems in the eutectic composition were prepared and further solid-state characterized using powder X-ray diffraction (PXRD), Fourier transform infrared spectroscopy (FT-IR), scanning electron microscopy (SEM), and contact angle measurements, as well as solubility and powder dissolution tests. In addition, intermolecular interactions in solution between the constituents of the three eutectic systems were studied through ^{1}H and ^{13}C nuclear magnetic resonance (NMR).

MATERIALS AND METHODS

Materials

Piperine (PIP) and curcumin (CUR) were obtained and isolated from *Piper nigrum* and *Curcuma longa* respectively at the BIODESS laboratory. Lovastatin (LOV) was purchased from Valdequimica, Brazil (purity reported > 99%), and irbesartan (IBS) was kindly donated by CALOX of Costa Rica in its micronized form A. CUR, LOV, IBS, and PIP analytical standards were purchased from Sigma-Aldrich from Laramie, WY, USA. These reference substances were used in the HPLC quantification studies. All solvents were HPLC/UV grade, and water was purified using a Millipore system filtered through a Millipore 0.22 µm Millipak™ 40 membrane.

Piperine Eutectic Mixture Screening

To evaluate the formation of eutectics between PIP and the selected substances, a 1:1 molar ratio binary mixture was prepared to combine CUR-PIP, LOV-PIP, and IBS-PIP in the corresponding weight to obtain 15 mg of each mixture. Then, the mixtures were ground together, assisted with 20 µL of ethanol in a glass mortar, and pestle for around 10 min or until the solid was dried entirely. Approximately 2 mg of the mixture was placed into an aluminum crucible and analyzed from 40

to 200 °C at a heating rate of 10 °C/min using the DSC equipment described in the following sections. The schematic representation of the process is illustrated in Fig. 3.

Determination of Mixture Composition at the Eutectic Point

The composition at the eutectic point of each mixture was obtained by the construction of Tammann's and binary phase diagrams. The diagrams were arranged following the recommendations proposed by the literature (27, 28). Special attention was given to the use of DSC data suggested by Rycerz, 2013 (29). Firstly, different molar ratios (e.g., 0.1:0.9, 0.2:0.8 to 0.9:0.1) of each EM were prepared to place the appropriate amount of each component to obtain 10 mg of the desired binary mixture composition. The homogenization and DSC analyses of each molar ratio were followed as described in the previous section. In the phase diagram construction, the onset temperature of the first endothermic event was used as the solidus point, and the peak of the second endothermic event was considered the liquidus point. Thermal events observed in DSC can be determined as the starting variation of the baseline, at the maximum peak or in the intersection from the baseline with the extension of the line tangent to the peak, commonly known as onset temperature (30, 31). In general, the onset temperature is preferred (30, 31) because reports indicate this value is less affected by the variation in the heating rate (32). Therefore, in the Tammann diagrams, the onset temperature, and the enthalpy of fusion of the first endothermic event were used as employed by Höhne *et al*. (2003) (30) and by Rycerz (2013) (29). Data analyses were performed using TA Instruments-Waters LLC Universal Analysis 2000 software (version 4.5A, New Castle, DE, USA, 2016). Each analysis was performed in triplicate.

Preparation of Bulk Mixtures at the Eutectic Composition

Bulk material of each EM was prepared in their respective eutectic composition to characterize the CUR-PIP, LOV-PIP, and IBS-PIP systems deeply. One gram of each EM was prepared based on the method described in the previous section using the eutectic composition derived from binary phases and Tammann's diagrams. Appropriate amounts of each drug and PIP were accurately weighed to obtain CUR-PIP at 0.41:0.59, LOV-PIP 0.29:0.71, and IBS-PIP 0.31:0.69.

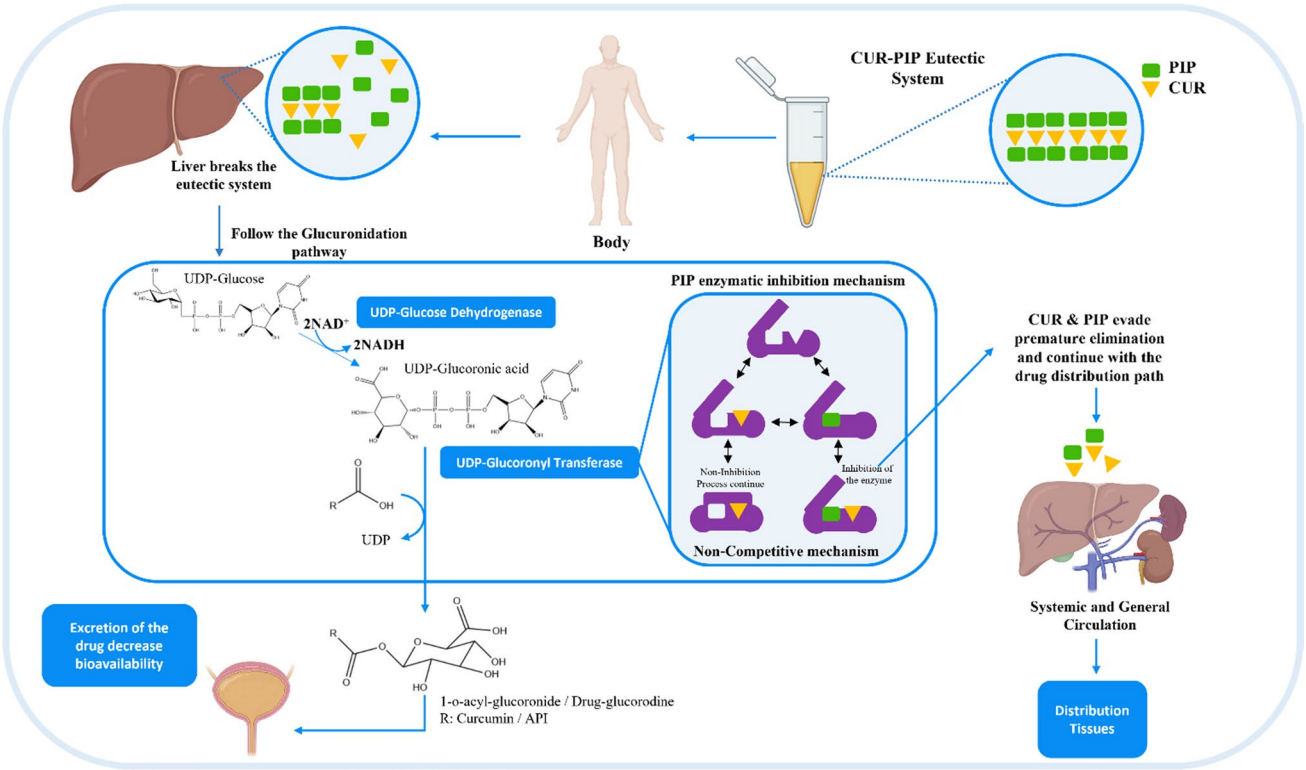

Fig. 1 Illustrated scheme for the glucuronidation mechanism to prevent early excretion of drugs, applied to CUR-PIP system to increase CUR solubility and bioavailability (figure created with BioRender.com). Figure adapted from the previously reported mechanisms (24, 25)

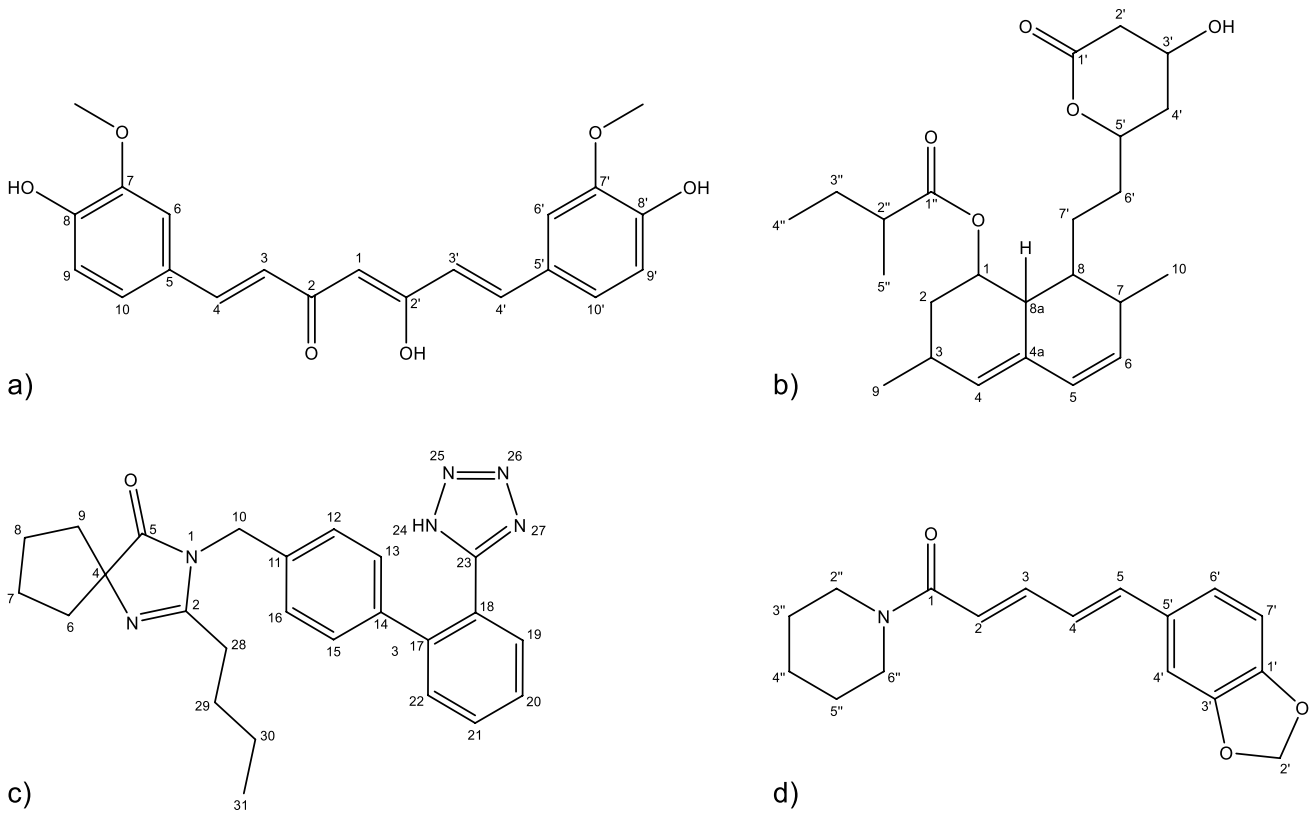

Fig. 2 Chemical structure of **a** curcumin (CUR), **b** lovastatin (LOV), **c** irbesartan (IBS), and **d** piperine (PIP)

The mixtures were homogenized in a glass mortar and pestle for nearly 20 min using 400 µL of ethanol as a catalyst. The obtained materials were dried at 60ºC for 1 h and stored in a desiccator until further analysis.

Thermal Analysis by DSC

Differential scanning calorimetry (DSC) analysis of the obtained eutectic solids was acquired using a DSC-Q200 (TA Instrument, New Castle, DE, USA) equipped with a TA Refrigerated Cooling System 90. For each sample, 2 mg was filled in aluminum pans. The measurement was executed under a dynamic nitrogen atmosphere with a 50 mL/min flow rate. The sample pans were heated at a rate of 10 °C/min from 40 to 200 °C using an empty standard aluminum pan as reference.

FT-IR

Fourier transform infrared (FT-IR) analyses were performed and recorded on a Thermo Scientific Nicolet 6700 FT-IR spectrometer fitted with a diamond attenuated total reflectance (ATR) accessory. The data were collected from 4000 to 600 cm^{-1} using 32 scans at 4 cm^{-1}. The samples were placed directly into the ATR cell without further preparation.

PXRD

The powder X-ray diffraction (PXRD) analysis was carried out in a PANalytical Empyrean diffractometer using a PIXcel detector (Medipix2). Samples were scanned in a zero-background sample holder with a copper tube (λ = 1.54 Å), 45 kV, 40 mA and scanning from 4° to 40°. A soller of 0.04 rad located at the X-ray tube and a large soller of 0.04 rad located at the detector were used. A divergence slit of 1/4° and antiscatter slit of 1/2° were implemented. Kβ was filtered by using Nickel. The software Data Collector, High Score plus and PDF4 + (2021) were utilized.

SEM

The morphology and crystal size of CUR, LOV, IBS, and PIP and the respective eutectic solids were determined using a JEOL JSM-6390 LV scanning electron microscope, the acceleration voltage applied was 20 kV. The samples were attached, mounted on a metal stub using double-sided

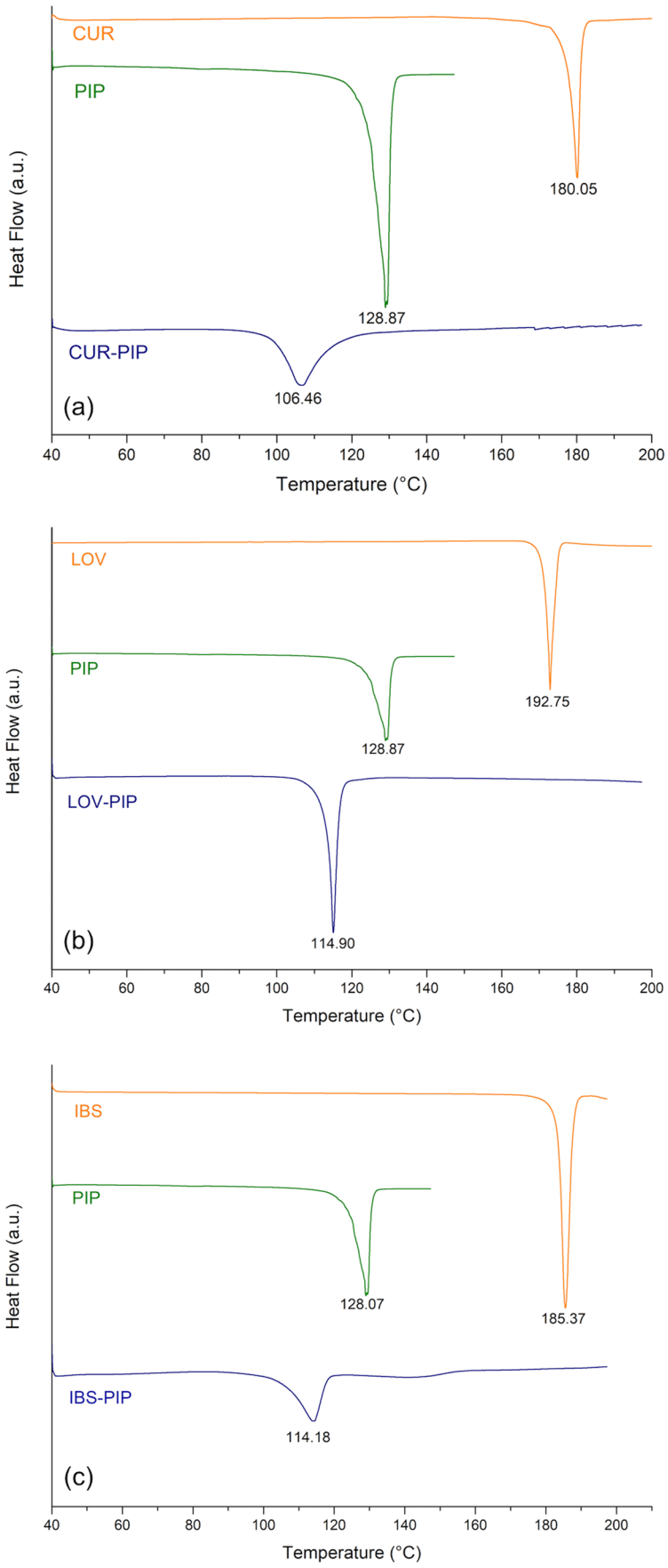

Fig. 3 DSC curves obtained in the EM screening. **a** CUR, PIP, and CUR-PIP. **b** LOV, PIP, and LOV-PIP. **c** IBS, PIP, and IBS-PIP. All binary mixtures at 1:1 molar ratio

adhesive tape, and coated under vacuum with gold in an argon atmosphere.

Contact Angle Measurement

Contact angle measurement was performed by the sessile drop technique using a Ramé-hart 250 F1 goniometer system and water as a solvent; the capture of the image and determination of the contact angle was carried out using the Drop-Image software.

Solubility Test

Aqueous solubility of pure CUR, LOV, IBS as well as in each EM system in their exact eutectic composition (i.e., CUR:PIP 0.41:0.59, LOV:PIP 0.29:0.71, and IBS:PIP 0.31:0.69) was performed placing an excess of the solids to 1.5 mL of pre-equilibrated water at 37.6 °C in 2.0-mL microtubes. Then, the microtubes were placed on BIOSAN TS-100C Thermo-Shaker (Riga, Latvia) at the constant stirring of 900 rpm and temperature of 37.6 °C for 72 h to achieve equilibrium. Subsequently, the samples were centrifuged at 6000 rpm in a Thermo Scientific Sorvall ST 16R centrifuge, maintaining the evaluation temperature. The solutions were then filtered through a 0.45 µm cellulose acetate filter membrane using a Sartorius stainless-steel syringe filter holder, and to determine drug content, solutions were analyzed by UPLC system described in Sect. 2.12.

Powder Dissolution Test

The dissolution tests of powder samples of pure drugs as well as in the EM in their exact eutectic composition (i.e., CUR:PIP 0.41:0.59, LOV:PIP 0.29:0.71, and IBS:PIP 0.31:0.69) were performed using the United States Pharmacopeia (USP) paddle method on a SOTAX S7 dissolution test system. The dissolution media for the studied drugs were selected accordingly to the USP monograph taking special attention to the use of high concentrations of surfactants (33) that could not discriminate changes in the solid state (34, 35). Therefore, phosphate buffer (PB) pH 7.4 was used to evaluate LOV, sodium lauryl sulfate (SLS) 0.25% to assess CUR and HCl 0.1 N for IBS. Each media was previously heated at 37 ± 0.5 °C, and the rotation speed was 50 rpm for LOV and IBS and 100 rpm for CUR, as indicated in the USP method. Five milliliters of the samples were withdrawn at specific time intervals replacing with the same volume of preheated fresh medium to ensure sink condition. The sample aliquots were filtered using a 0.45 µm cellulose acetate membrane placed into a Sartorius stainless-steel syringe filter holder and injected to determine drug concentration.

Determination of Drug Content

To analyze the drug content in the solubility and dissolution tests, a UPLC-DAD system composed of a Thermo Scientific™ UltiMate™ 3000 UHPLC equipment with variable wavelength detector, pump, variable temperature compartment column, and an autosampler was used. The chromatographic separation of LOV, CUR, IBS, and PIP simultaneously was achieved by modifying a previously reported method (36). Briefly, a Nucleosil 100-5C18 column (250 mm × 4.0 mm, 5 µm packing) with 1.0 mL/min rate flow, maintained at 37.5 ºC using a mobile phase composed of acetonitrile:phosphoric acid 0.1% using a gradient elution starting at 45:55 to reach 65:35 in 20 min. The detection and quantification were performed at 235, 420, and 280 nm for LOV, CUR, and IBS, respectively.

Solution-State NMR Spectroscopy

The ^{1}H NMR and ^{13}C NMR for the pure compounds PIP, CUR, LOV, and IBS, as well as for the three eutectic mixtures CUR-PIP, LOV-PIP, and IBS-PIP were performed on 12 mg of each sample in 0.5 mL of solvent in a Bruker Ascend 400 MHz instrument. Chemical shifts (δ) are reported in ppm relative to internal tetramethylsilane (TMS, $\delta = 0.0$ ppm) as standard. DMSO-*d*6 mixed with D_2O at a ratio of 9:1 (v/v) was used as a solvent due to the limited solubility of the molecules in water (37–39).

RESULTS AND DISCUSSION

EM Screening

Differential Scanning Calorimetry is the appropriate technique to perform a quick screening of the eutectic formation because the structural organization in eutectics based on the inhibition in crystallization of one another produces a significant reduction in the melting temperature compared with their parent compounds when a material is subjected to thermal analyses (40, 41). DSC curves of individual substances CUR, PIP, LOV, and IBS along with the 1:1 CUR-PIP, LOV-PIP, and IBS-PIP binary mixtures are shown in Fig. 3. The presence of a unique endothermic event at lower temperature than the starting materials is an indicative of EM formation. However, further characterization is required in order to confirm their formation.

The melting point is related to the intermolecular interactions in the crystalline structure determining the thermodynamic functions such as free energy, enthalpy, and entropy

of a material (42–44), which in turn affects the microstructure and consequently the physicochemical properties (43, 45).

Ideal EM do not interact to form a new chemical entity; however, weak inter-phase boundaries permitted atoms to diffuse and redistribute in the solid (46). The results are attributed to dispersion forces, and the eutectic point refers to the molar ratio at which a single melting temperature is observed for all components, and that temperature is minimal for the EM (46). Table I are presented the melting temperatures of the eutectic systems obtained. The properties exhibited by EM can significantly affect parameters such as the solubility and dissolution rate of crystalline solids in water (47). Hence, the exact composition at the eutectic point, the solid-state characterization, and other physicochemical properties were performed for the CUR-PIP, LOV-PIP, and IBS-PIP systems.

Binary Phase and Tammann Diagrams

Binary phase and Tammann diagrams were constructed for each eutectic system CUR-PIP, LOV-PIP, and IBS-PIP using DSC data from a series of melting endotherms of the binary mixtures obtained in variable molar ratios of CUR, LOV or IBS and PIP. Figures 4a, 5a, and 6a show these curves for the CUR-PIP, LOV-PIP, and IBS-PIP, respectively. Figures 4a and 5a, for CUR-PIP and CUR-LOV respectively showed two melting endotherms at high molar ratios (0.6, 0.7, 0.8, 0.9), whereas in the case of IBS-PIP in Fig. 6a, a single melting endotherm was observed along all molar ratios studied. Two melting endotherms is related to the non-ideal behavior of the EM in which the first event is the EM point and the second corresponded to the melting of the compound that remains in excess after eutectic formation (48). This phenomenon did not occur in the IBS-PIP system, in which only one endothermic is observed at several molar ratios. This could indicate that this system behaves as an ideal system suggesting that the PIP has better miscibility with IBS than with CUR and LOV.

In the phase diagram construction, the onset temperature of the first endotherm of the DSC curve was used as the solidus point and the peak temperature of the second endotherm as the liquidus point. Moreover, the Tammann diagram shows the systematic dependence of molar enthalpy associated with the eutectic effect on the mole fraction (29). Therefore, several authors use molar ratio in the construction of Tammann's diagrams (49–51) while others prefer mass percent (52). Figures 4b, c, 5b, c, and 6b, c present both diagrams for each studied eutectic system. The eutectic composition obtained from these diagrams for the three systems is presented in Table I.

Solid-State Characterization of EM in Their Respective Eutectic Composition

EM formation is based on the minimum composition of two or more solid components that during the crystallization process, a mixture of the component acts as a single component (53). The crystalline structures in an EM remain unaffected from the original components, except for the disorder introduced during the formation. Based on the melting properties of the pure components, the EM can have a defined microstructure formation compared to the physical mixture (41). Various physical properties of the eutectic materials depend on their microstructures; the solidification of the liquid phase of the eutectic material is a complex process that depends upon the solidification dynamics and concentration phase separation (54), the intermolecular forces with a significant presence of electrostatic interactions (8). The main interactions involved in the EM formation are expected to occur between the carbonyl, hydroxyl, and amine groups in CUR, PIP, LOV, and IBS. Therefore, a complete characterization was conducted, which is presented in the following sections.

PXRD and FT-IR Analyses

Powder X-ray diffraction (PXRD) and FT-IR analyses were performed to determine crystalline forms in the samples as a qualitative indicator of the crystallinity and to detect interactions between PIP and the studied drugs. PXRD shows any modification of the crystalline structure undergone in the eutectics formation process, while FT-IR shows the vibrational modes due to the intermolecular forces that occur in the solid-state and if the eutectic form presents structural, conformational or environmental modifications (28, 55). Further, in the formation of EM, the resulting solid could also present molecular associations drug-drug and coformer-coformer, which however should not produce new signals in the PXRD or shifts with considerable deviations in the FT-IR (49).

PXRD patterns in Fig. 7 for all three systems indicate that the parent solids and the material obtained from the process of the binary mixture are crystalline. All the reflections in

Table I Eutectic Temperature and Composition of the Three Eutectic Systems

System	Eutectic temperature (±SD, °C, $n=3$)	Eutectic composition (molar ratio)
CUR-PIP	106.92 ± 0.07	0.41: 0.59
LOV-PIP	115.07 ± 0.10	0.29: 0.71
IBS-PIP	119.68 ± 0.14	0.31: 0.69

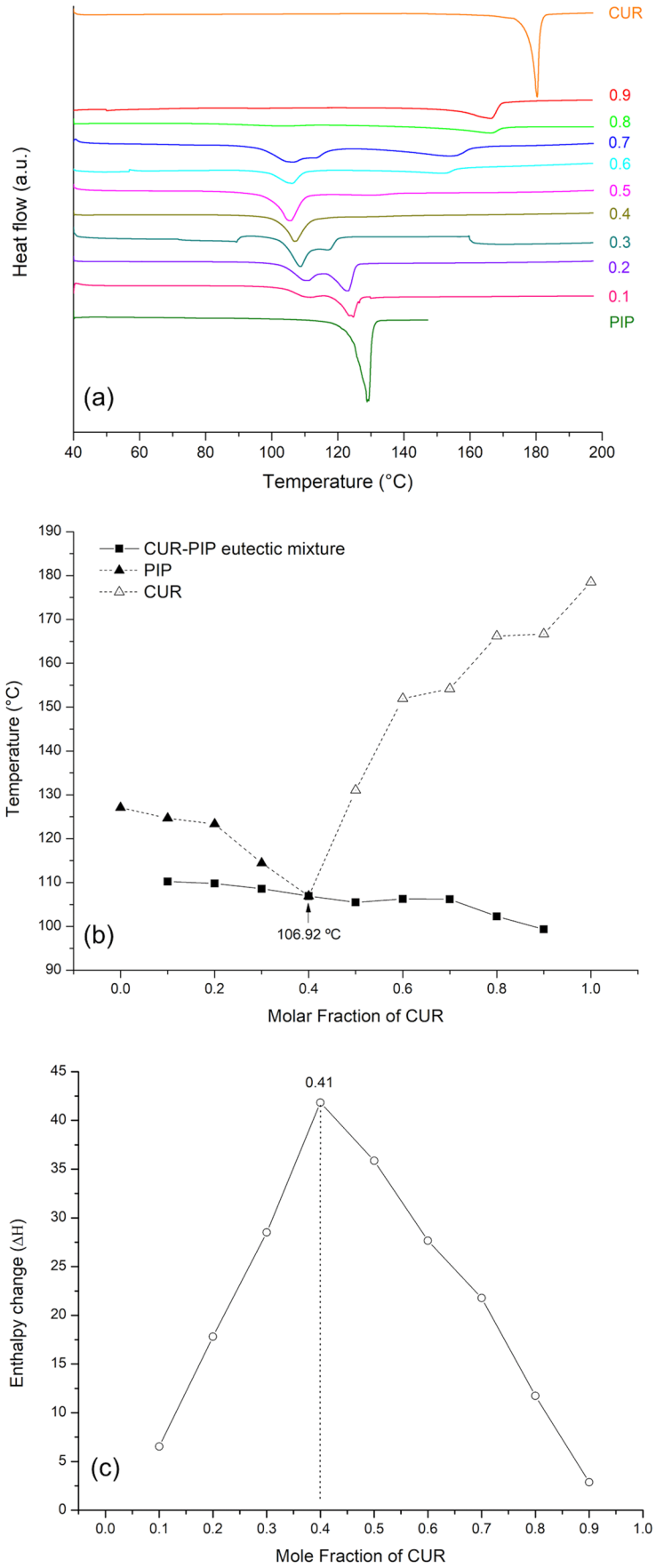

Fig. 4 **a** DSC curves used to construct **b** the eutectic phase diagram where filled triangle and empty triangle represent the variable liquidus line, and filled square represents the solidus line. **c** The Tamman diagram of CUR-PIP EM

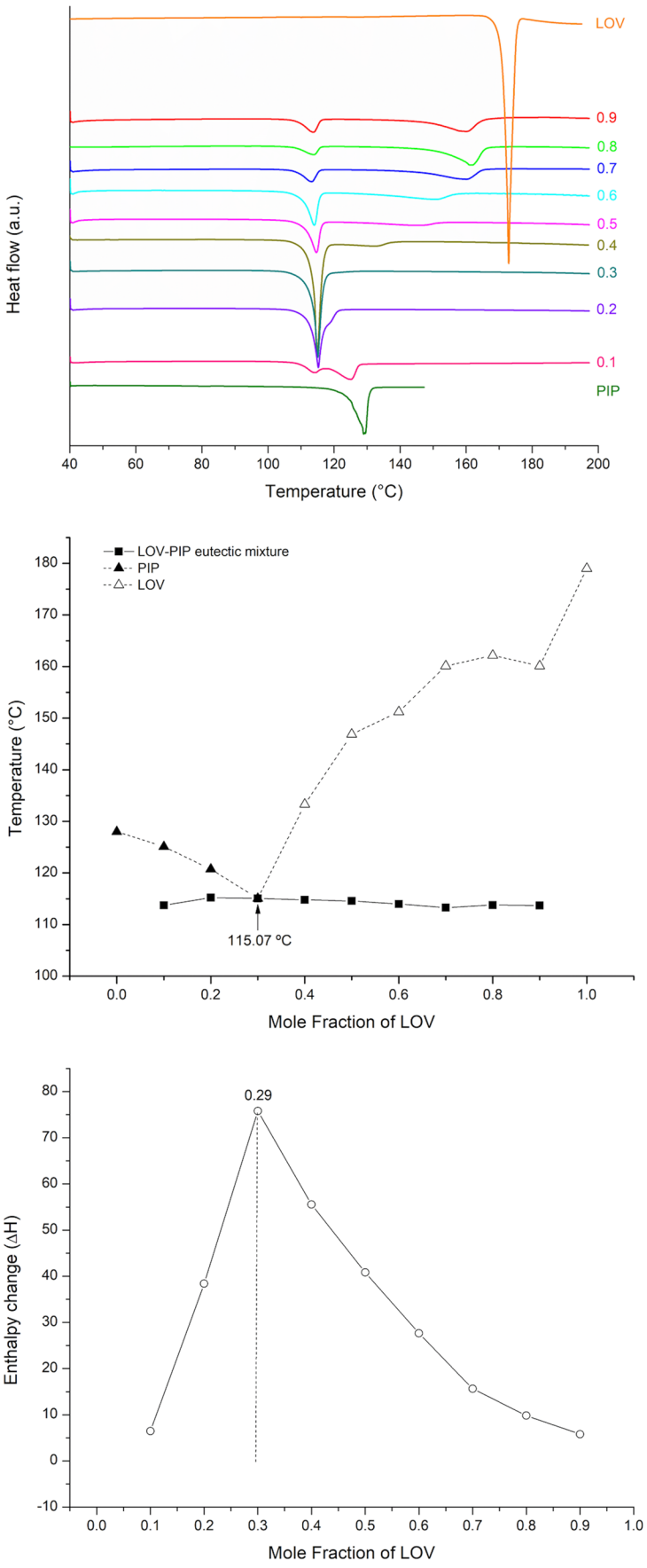

Fig. 5 **a** DSC curves used to construct **b** the eutectic phase diagram where filled triangle and empty triangle represent the variable liquidus line, and filled square represents the solidus line. **c** The Tammann diagram of LOV-PIP EM

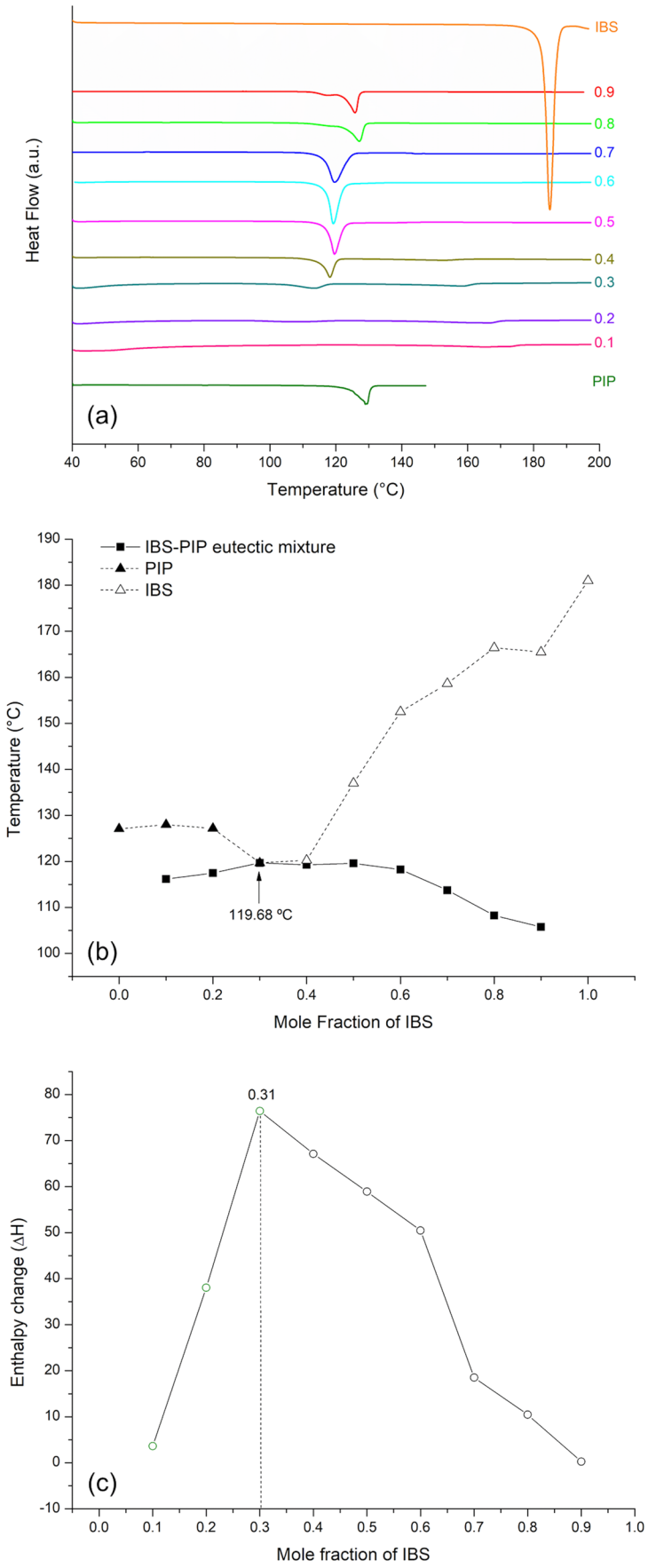

Fig. 6 **a** DSC curves used to construct **b** the eutectic phase diagram where filled triangle and empty triangle represent the variable liquidus line, and filled square represents the solidus line. **c** The Tamman diagram of IBS-PIP EM

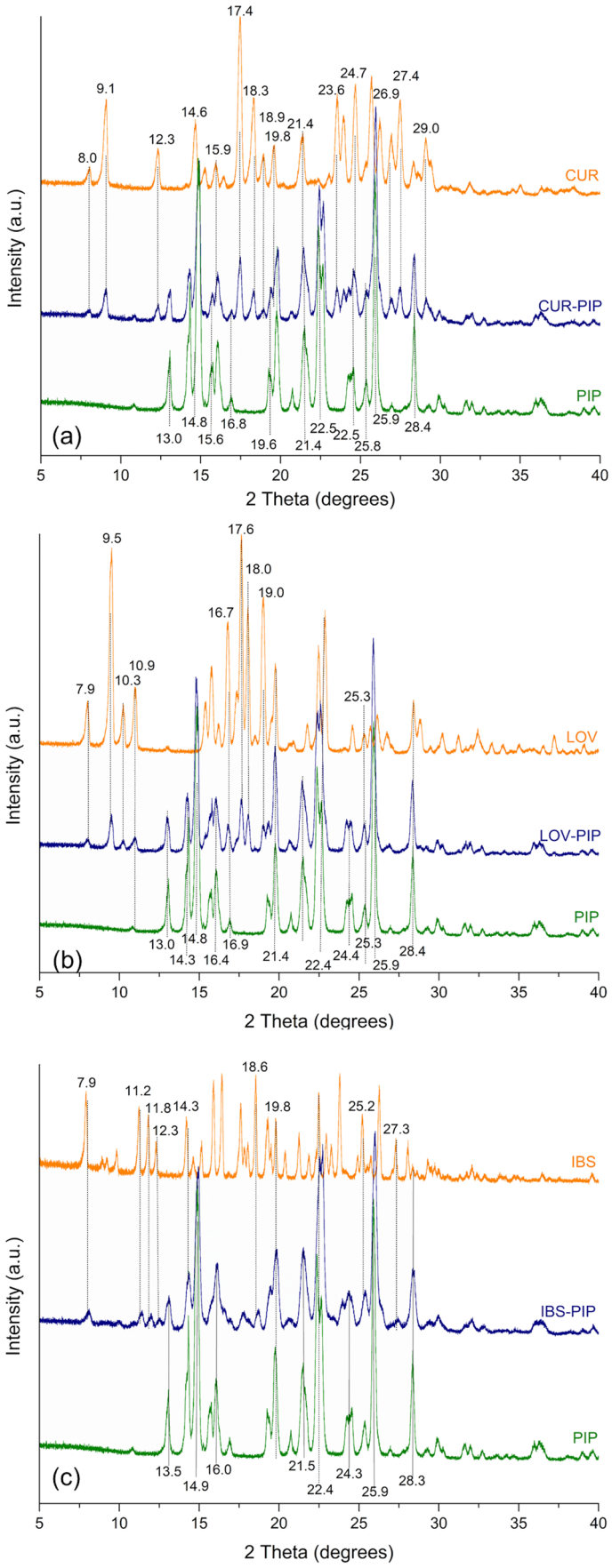

Fig. 7 PXRD of the eutectic systems CUR-PIP at 0.41:0.59 molar ratio, LOV-PIP at 0.29:0.71 molar ratio, and IBS-PIP at 0.31:0.69 molar ratio and their pure constituents

the pattern of the binary mixtures are present in their respective pure components, indicating no formation of a new crystalline phase; this is an indicator of the weaker interactions in the solid state. Decreases in reflections' intensity observed for all the system, however, more evident in the CUR-PIP system can be attributed to the amorphization of the EM caused by the grinding process. For this system, the most relevant peaks 12.2, 17.4, 18.3, and 27.4 were present in the EM and the pure CUR, besides the most relevant peaks from PIP were 14.3, 14.8, 22.4, and 26.0. For the system LOV-PIP, the most significant peaks were 7.9, 9.5, and 26.8 are present in the EM and the pure LOV, as well the most relevant peaks from PIP were 12.9, 14.8, 19.8, and 25.9. For the system IBS-PIP, the major peaks were 14.2 and 13.1 are present in the EM and the pure IBS, as well the most significant peaks from PIP were 14.8, 22.5, and 25.9. These results, along with the obtained from the DSC data, confirm the EM formation.

FT-IR spectroscopy can detect molecular interactions, for instance, the hydrogen bond formation is commonly observed as a broader band and increased wavenumber position related to X–H bending and in a lower position associated with the carbonyl C = O stretching (56). In this regard, according to the molecular synthon theory (57–59), there are potential interactions between drug and coformer in the studied systems, such as intermolecular hydrogen bonds between the carbonyl group in PIP and the OH groups in CUR and LOV or the N–H group of the tetrazole ring in IBS. The presence or absence of these interactions defines the type of MOM formed. Figure 9 presents the FT-IR spectra of the EM and their respective pure components, which contain the most relevant signals ranging from 1800 to 800 cm^{-1}. The complete FT-IR spectra of the EM and their respective pure components is presented in Fig. S1.

The FT-IR of PIP showed characteristic bands at 2939 cm^{-1} corresponding with the -CH stretching of the benzene ring; at 1582 cm^{-1} related to the asymmetric bend of the carbonyl group (O = C–N); at 1491 cm^{-1} associated with aromatic (-C = C-) stretching; at 1430 cm^{-1} assigned to -CH_2 bending and at 1252 cm^{-1} to -C-O stretching (60, 61).

Characteristic CUR signals were observed at 3313 cm^{-1} (alcohol -O–H stretching), 2921 cm^{-1} (methyl -C–H asymmetric stretching), 1626 cm^{-1} (-C = O stretching), 1455 cm^{-1} and 1427 cm^{-1} (-CH_2 bending), 958 cm^{-1} (alcohol -C–OH stretching) (61). Meanwhile, CUR-PIP EM spectrum shows similar peaks positions at 3310 cm^{-1} (alcohol -O–H stretching), 2921 cm^{-1} (methyl -C–H asymmetric stretching), 1635 cm^{-1} (-C = O stretching), 1579 cm^{-1} corresponding to asymmetric bend of the carbonyl group (O = C-N), and 1251 cm^{-1} to -C-O stretching, both signals observed in the PIP spectrum. Therefore, the FT-IR spectrum of CUR-PIP EM resulted in the summation of the absorption bands described for CUR and PIP individually.

LOV FT-IR spectrum showed intense absorption bands at 3538 cm^{-1} (alcohol -O–H stretching), 2964 cm^{-1} (methyl -C-H asymmetric stretching), 2924 cm^{-1} (methylene -C-H asymmetric stretching), and 2871 cm^{-1} (methyl and methylene -C-H asymmetric stretching). In addition, bands at 1696 cm^{-1} (lactone and ester -C = O stretching), 1491 cm^{-1} (aromatic -C = C- stretching), 1259 cm^{-1} (-C-O stretching), 1116 cm^{-1} (lactone -C–C symmetric bend), and 966 cm^{-1} (alcohol -C–OH stretching) (62). Absorption bands in LOV-PIP EM included these signals and others at 1582 cm^{-1} and 1490 cm^{-1} corresponding to PIP asymmetric bend of the carbonyl group (O = C-N) and aromatic -C = C- stretching, respectively. Thus, as can be observed in Fig. 8, the LOV-PIP EM spectrum exhibited the signals of the individual components without any considerable shifting for their main functional groups.

Similar observations were exhibited by the IBS-PIP system shown in Fig. 8. The characteristic absorption peaks of IBS were found at 2957 cm^{-1} (-N–H stretching), 1729 cm^{-1} (-C = O stretching), and 1406 (-C = C- stretching). Those IBS characteristic peaks were also present in the IBS-PIP EM FT-IR spectrum. The peak at 1614 cm^{-1} corresponds to the asymmetric bend of the carbonyl group (O = C–N) which is present in IBS, IBS-PIP EM, and PIP. Hence, in IBS-PIP EM, the absorption band at 1253 cm^{-1} (-C-O stretching) belongs to the signal present in PIP.

In sum, the FT-IR and PXRD results supported that there was no strong chemical interaction between PIP and the model drugs in the solid-state. Consequently, the resulting eutectic microstructure matches with the lattice structures of the parent components as phase-separated domains (crystalline solid solutions) (63).

SEM

SEM images accurately contrast the morphological characteristics of drugs and the selected coformer, which have manifestly distinct morphology, provide a valuable tool in identifying the eutectics as separate entities from their parent drug (49). The SEM micrographs of individual components and EMs are presented in Fig. 9. PIP in Fig. 9 a and b showed tabular closely spaced as observed for hesperetin by Chadha *et al.* (2017) (27) of about 20–10 µm in size. Similar morphology was exhibited by IBS in Fig. 9e with size ranging from 5 to 10 µm. Further, Fig. 9 c and d presented CUR and LOV respectively both showed small irregular sharp-edged crystals similar to those observed in theobromine crystals reported by the same authors (27) of roughly 20–10 µm size. The crystals of LOV-PIP and IBS-PIP represented in Fig. 9f–h shows similar irregularly clusters morphology with no well-defined shaped of crystals ranging in size from 10 to 20 µm.

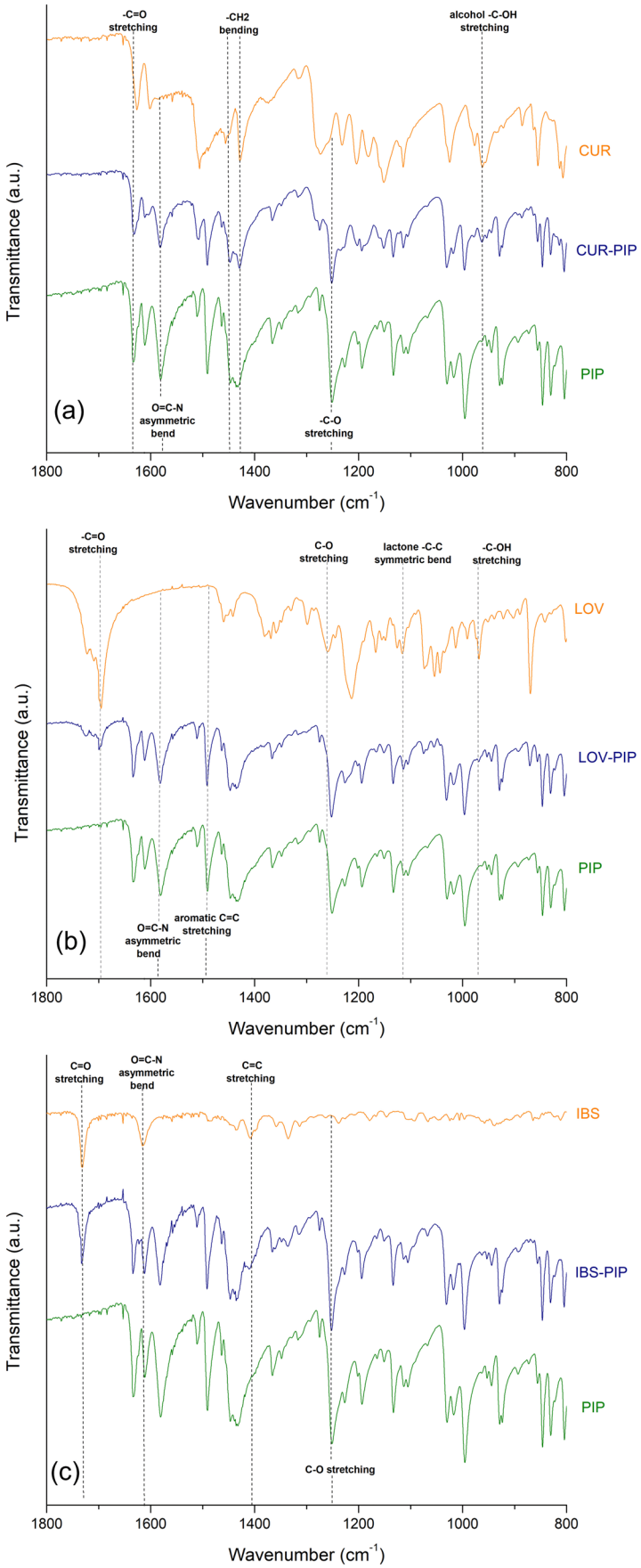

Fig. 8 FT-IR spectra in the range of 800 to 1800 cm^{-1} of the CUR-PIP, LOV-PIP, and IBS-PIP eutectic systems and their pure constituents (see the supplementary material for the complete range of the FT-IR spectra)

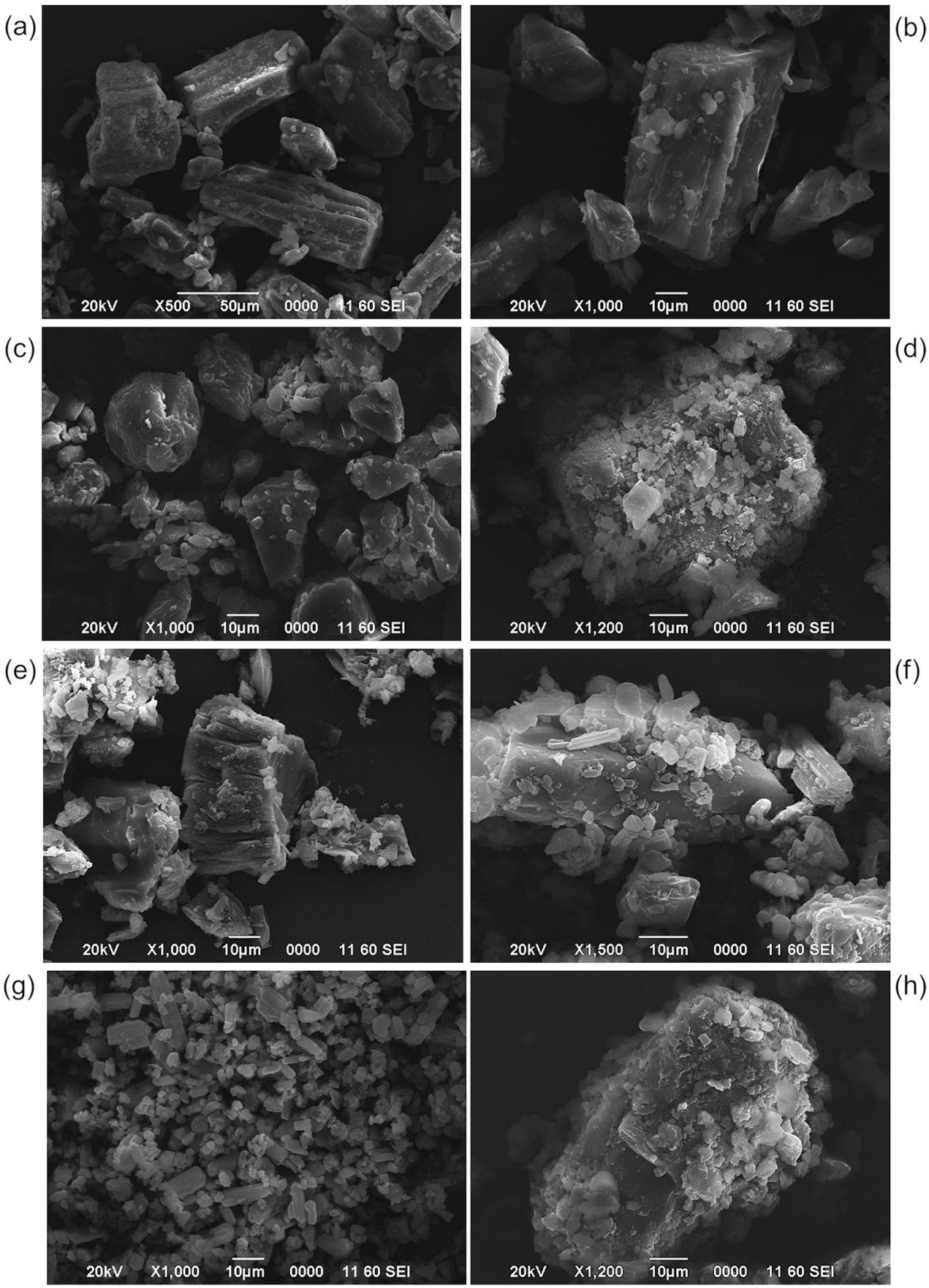
(a)
20kV X500 50µm 0000 11 60 SEI
(b)
20kV X1,000 10µm 0000 11 60 SEI
(c)
20kV X1,000 10µm 0000 11 60 SEI
(d)
20kV X1,200 10µm 0000 11 60 SEI
(e)
20kV X1,000 10µm 0000 11 60 SEI
(f)
20kV X1,500 10µm 0000 11 60 SEI
(g)
20kV X1,000 10µm 0000 11 60 SEI
(h)
20kV X1,200 10µm 0000 11 60 SEI

◂**Fig. 9** Micrographs of **a**, **b** pure PIP, **c** pure CUR, **d** pure LOV, **e** pure IBS, and the binary mixture at the eutectic composition: **f** CUR-PIP, **g** LOV-PIP, and **h** IBS-PIP

Contact Angle Measurements and Aqueous Solubility Test

The EM preparation strategy is intended to increase the water solubility (28, 42, 49, 64) of the selected low aqueous soluble drugs LOV, IBS, and CUR, which limit their bioavailability compromising their beneficial effects. Therefore, both the contact angle and the solubility tests were performed using water as a medium.

According to literature reports, the water solubility of CUR, IBS, and LOV at 25 °C are 3.12 mg/L (20), 0.059 mg/L (39), and 0.059 mg/L (38), respectively. The variation observed in the values determined herein at 37 °C can be attributed to the difference in solubility exhibited by drugs polymorphs (65, 66), which are not considered in those literature reports. On the other hand, LOV's solubility reported by Patel *et al*. (2008) (67) is consistent with the values determined in this study for a drug that has not presented polymorphism (68).

Contact angle measurements of CUR-PIP, LOV-PIP, and IBS-PIP EMs, with their respective pure components CUR, LOV, and IBS, and the aqueous solubility values of powdered samples are shown in Table II.

In the three eutectic systems, contact angle values decreased while the aqueous solubility increased compared to their respective pure molecule of interest. In this scenario, contact angle corresponds to the degree of wettability when a liquid interface meets a solid surface. The smaller contact angle indicates higher wettability, which implies a more hydrophilic surface and can thus result in better dispersibility in the medium. As the liquid drop touches the solid surface, the hydrophilic eutectic components act as a dissolved solid surface in the liquid–solid interface to reduce contact angle (50). Higher wettability also implies that a powder has low surface tension or higher surface energy; therefore, a highly wetted sample tends to dissociate easily in water. Both results suggested that one of the factors involved in the improvement in aqueous solubility was the higher wettability of powdered samples. In the specific case of IBS when the decreased in contact angle was no proportional to the improvement in solubility, there would be other factor influencing the improvements in solubility.

Other multicomponent systems containing IBS have been reported in the literature showing variable improvements in solubility (30). For instance, the improvement for IBS-benzoic salt and IBS-piperazine salt solubility were 3.3- and 367.3-fold compared to IBS form A, respectively. Therefore, the enhancement in solubility exhibited by the IBS-PIP system is promising to consider an EM is not a new chemical entity.

Powder Dissolution Test

In vitro dissolution test is a valuable tool for the excipient selection during the pharmaceutical development process and to evaluate the dissolution characteristics of the drug product (69–71). The ideal dissolution media for the test is water or biorelevant media (72). However, considering the poor water solubility of many drugs, the use of surfactants becomes necessary. Special attention should be given to their use to enable the dissolution media to detect significant differences in the *in vitro* and *in vivo* performance of the drug (34, 35).

The selection of the dissolution media was based on the USP monograph for each drug dosage form. The dissolution media for IBS tablets is HCl 0.1 N, for curcuminoid tablets is 1% of sodium lauryl sulfate (SLS), and for LOV tablets is phosphate buffer containing approximately 2% of SLS and pH adjusted to 7 using 1 N sodium hydroxide. It should be noted that high concentrations of surfactants (33) would not allow to discriminate of changes in the solid state (34, 35). Regarding the use of SLS, some reports show anomalous dissolution profiles corresponding to salt or complex formation between the drug and SLS (73–75). On the other hand, SLS at 0.25% has been previously used allowing to distinguish between polymorphs (76) and to assess differences in crystalline domain size of raw material batches (77). Therefore, the dissolution media chosen were phosphate buffer (PB) pH 7.4 to evaluate LOV, SLS 0.25% to assess CUR and HCl 0.1 N for IBS.

The dissolution profiles of pure powdered compounds and their EMs are shown in Fig. 10. LOV dissolution profile in pH 6.8 phosphate buffer has been reported by Madhuri *et al*. (2020), with less than 5% of the drug dissolved within 1 h, in a similar pattern that results shown Fig. 10b (78). In turn, findings reported for CUR by Rachmawati *et al*. (2013) using SLS 1% as dissolution medium accounted for 10% of the drug dissolved after 1 h, similar to results in the present study (79). Finally, data obtained in this study for IBS align with previous reports in the literature using the same dissolution media accounting for 30% and 40% of drug dissolution between 30 min and 1 h (80, 81), similar to data shown in Fig. 10c. An enhancement in the dissolution rate of the three molecules of interest in the EM was observed, which could be explained by the corresponding increase in solubility and wettability. For the first 5 min, the drugs' concentration was quite similar in their pure forms compared to EM. In CUR-PIP and LOV-PIP systems, the concentration increased over time, keeping a similar profile to pure CUR and LOV, respectively. In the IBS-PIP system, the dissolution profile of pure IBS was different from the one of IBS in the EM, which despite the significant IBS aqueous solubility enhancement in the EM, it could not be considered a burst dissolution behavior.

Table II Solubility and Contact Angle of the Three Eutectic Systems

System	Contact angle (±SD, °, $n=3$)	Aqueous solubility (±SD, mg/L, $n=3$)
Pure CUR	63.36 ± 0.22	1.42 ± 0.05
CUR-PIP	47.93 ± 0.74	7.85 ± 0.01
Pure LOV	50.37 ± 0.45	2.3 ± 0.2
LOV-PIP	33.25 ± 0.93	9.6 ± 0.6
Pure IBS	58.21 ± 0.02	1.2 ± 0.2
IBS-PIP	35.77 ± 0.39	140.4 ± 1.7

Solution-State ^{1}H NMR and ^{13}C NMR Spectroscopy

To obtain further evidence supporting in the EM of CUR-PIP, LOV-PIP, and IBS-PIP behavior in solution, NMR spectroscopy was used. The ^{1}H-NMR spectra for the three EM and the individual components are shown in Fig. 11. In addition, Table III summarizes the chemical shifts (δ) for each signal and also includes the induced chemical shift differences (Δδ), which were calculated as follows: Δδ = δ (pure drug)—δ (binary mixture), with the positive and negative signs showing upfield and downfield displacement, respectively. The number for each atom is shown in the chemical structures presented in Fig. 2.

Values obtained for chemical shifting (Δδ) show no significant differences, with a little change at the second decimal level, while larger changes would have been observed if a chemical change had occurred (50). Thus, indicating that binary EM of CUR-PIP, LOV-PIP, and IBS-PIP in solution state interact through intermolecular forces (82).

On the other hand, ^{13}C NMR spectroscopy analyses were performed to gain further insight into the intermolecular behavior in solution between the constituents of the EM. The ^{13}C NMR spectrum is shown in Fig. 12, while Table IV summarizes the chemical shifts (δ) for each signal and the induced chemical shift differences (Δδ), calculated as explained above.

Values obtained for chemical shifting (Δδ) in these ^{13}C NMR show no significant differences (< 1 ppm), indicating binary EM of CUR-PIP, LOV-PIP, and IBS-PIP in solution. The ^{13}C NMR displays the most significant changes in chemical shifts showing the regions of the molecules whit the strongest interactions in the EMs (64, 83).

For instance, the EM of CUR-PIP shows in the ^{13}C-NMR significant changes near the electronegative atoms of PIP. As shown in Table III, these changes occur for the aromatic carbons near the dioxymethylene group (C1', C3') as well as the dioxymethylene itself (C2'). Further, similar changes occur for the carbonyl (C1) and the adjacent vinylic group (C2, C3). In CUR, the primary shifting occurs in the center of the molecule near the carbonyls (C2, C3, C2', C3'), and a less significant shift occurs in the aromatic carbons near the methoxy group (C6, C7, C6', C7'). These changes agree with the regions near electronegative atoms, which are favorable for polar interactions (64).

In LOV-PIP EM, the aromatic ring and dioxymethylene group of PIP are again the signals with greater shifts, while for LOV, most carbons show minimal changes in the chemical shifts, except the olefinic carbons C4 and C5 and, to a lesser extent, the hydroxyl carbon C3' in the lactone ring. Again, the differences are located in electron-rich regions of LOV. Finally, IBS-PIP EM shows significant shifting in PIP's aromatic carbons, the dioxymethylene group and the central carbon chain (C1, C2, C5). In turn, IBS shows main chemical shifts changes in the tetrazole (C23) and the carbon C18 bonded to it, which is consistent with the previous explanation because of its highly electronegative nature. Another significant shifting is located in the carbonyl (C5) and, somehow less important, in the carbons of the lateral chain (C28, C30, C31), which would suggest hydrophobic interactions (64).

In addition, the changes in chemical shift are not significant in both ^{1}H NMR and ^{13}C NMR spectra, it was supposed that molecular interactions between PIP and three drugs in this solvent system would be useful for estimating molecular interactions that contribute to the increase in the solubility of

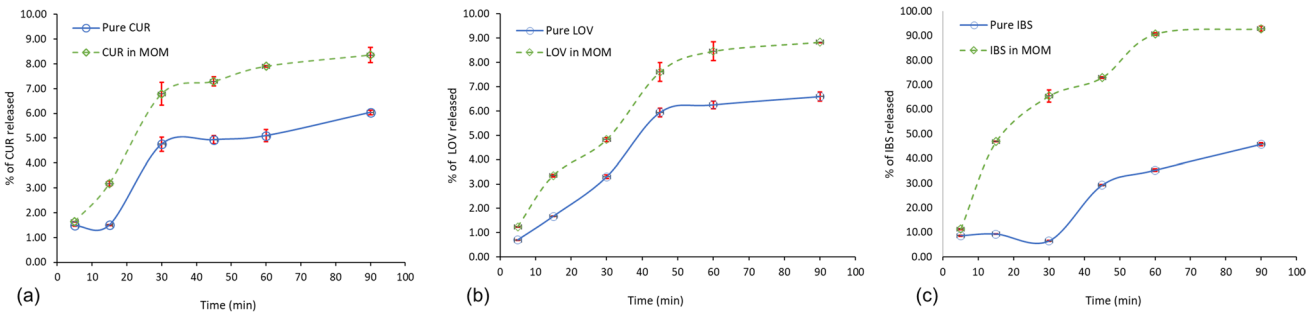

Fig. 10 Comparative dissolution profiles of each bioactive molecule and the binary mixtures in their eutectic composition: **a** CUR, **b** LOV, and **c** IBS

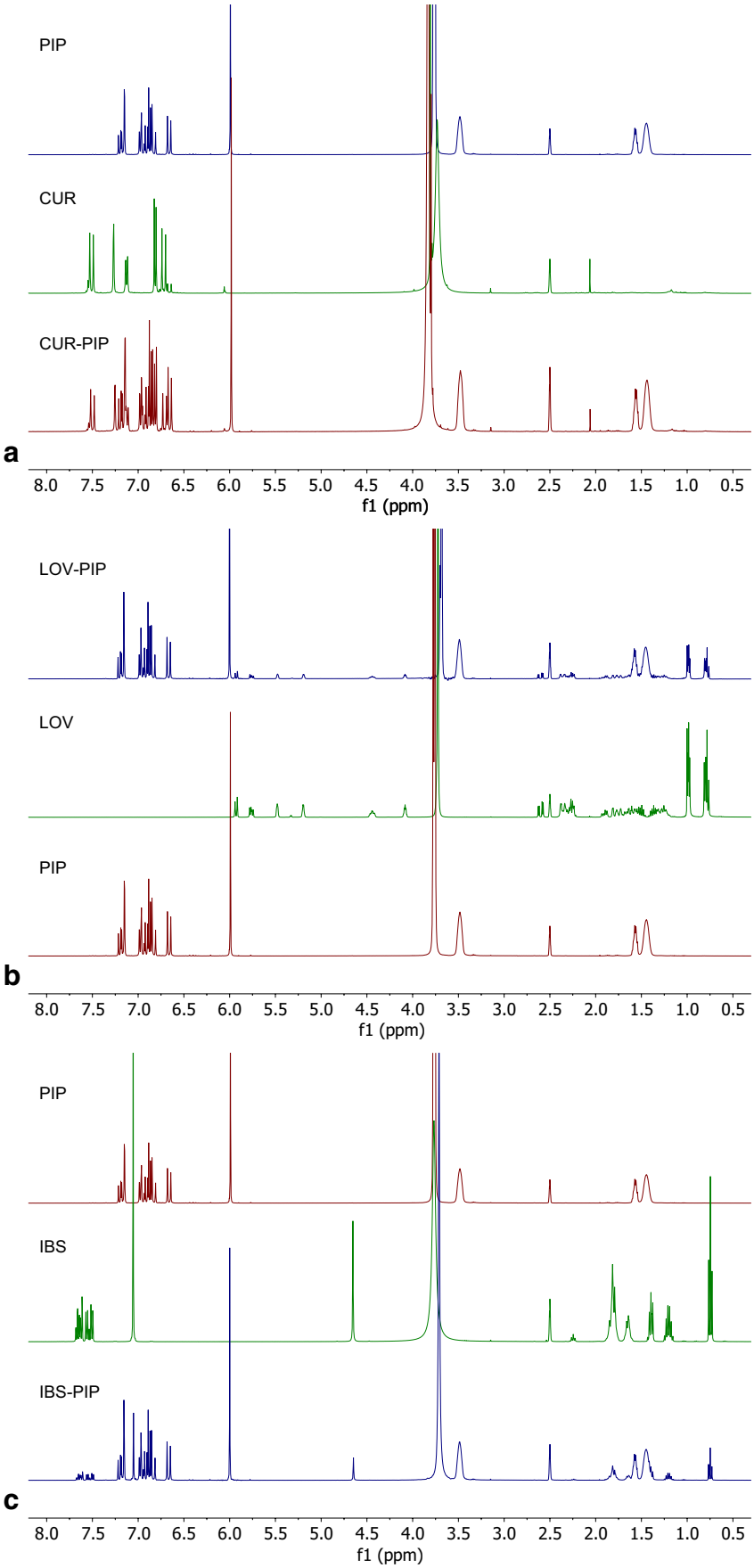

Fig. 11 Solution-state ^{1}H NMR of piperine (PIP) and **a** curcumin (CUR) and CUR-PIP, **b** lovastatin (LOV) and LOV-PIP, and **c** irbesartan (IBS) and IBS-PIP

Table III ^{1}H-NMR Chemical Shift Comparison Between EM and Their Constituents

	Pure compound[a]		$EM_{CUR-PIP}$		$EM_{LOV-PIP}$		$EM_{IBS-PIP}$	
	#H	δ (ppm)	δ (ppm)	Δ δ (ppm)	δ (ppm)	Δ δ (ppm)	δ (ppm)	Δ δ (ppm)
PIP signals	2	6.66	6.64	0.02	6.67	−0.01	6.66	0.00
	3	7.21	7.21	0.00	7.22	−0.01	7.22	−0.01
	4	6.97	6.96	0.01	6.98	−0.01	6.97	0.00
	5	6.87	6.92	−0.05	6.89	−0.02	6.87	0.00
	2'	5.99	5.98	0.01	6.00	−0.01	5.99	0.00
	4'	7.19	7.18	0.01	7.18	0.01	7.19	0.00
	6'	7.15	7.14	0.01	7.15	0.00	7.15	0.00
	7'	6.82	6.88	−0.06	6.81	0.01	6.83	−0.01
	2", 6"	3.49	3.49	0.00	3.45	0.04	3.49	0.00
	3", 5"	1.46	1.44	0.02	1.47	−0.01	1.45	0.01
	4"	1.56	1.56	0.00	1.54	0.02	1.57	−0.01
CUR signals	-OMe	3.73	3.79	−0.06				
	1	6.06	6.06	0.00				
	3, 3'	6.72	6.73	−0.01				
	4, 4'	7.55	7.54	0.01				
	6, 6'	7.27	7.25	0.02				
	9, 9'	6.81	6.83	−0.02				
	10, 10'	7.13	7.12	0.01				
LOV signals	1	2.50			2.50[b]	0.00		
	2	2.24			2.24	0.00		
	3	1.26			1.26	0.00		
	4	5.96			5.94	0.02		
	5	5.48			5.48	0.00		
	6	5.77			5.75	0.02		
	7	2.31			2.31	0.00		
	8	2.35			2.34	0.01		
	8a	4.45			4.43	0.02		
	9, 10	0.99			0.99	0.00		
	2'	2.59			2.60	−0.01		
	3'	4.07			4.08	−0.01		
	4'	1.90			1.90	0.00		
	5'	5.26			5.20	0.06		
	6'	1.38			1.36	0.02		
	6'	1.79			1.77	0.02		
	7'	2.38			2.38	0.00		
	2"	2.29			2.28	0.01		
	3"	1.50			1.52	−0.02		
	4", 5"	0.84			0.84	0.00		
IBS signals	6, 9	1.64					1.65	−0.01
	6,7,8,9	1.82					1.82	0.00
	10	4.66					4.63	0.03
	12,13,15,16	7.07					7.04	0.03
	19,21	7.64					7.63	0.01
	20,22	7.53					7.52	0.01
	28	2.25					2.23	0.02
	29	1.39					1.39	0.00
	30	1.19					1.20	−0.01
	31	0.75					0.75	0.00

[a]Signals correspond to pure PIP and pure drugs CUR, LOV, and IBS measured in independent experiments

[b]Under DMSO-d_6 signal

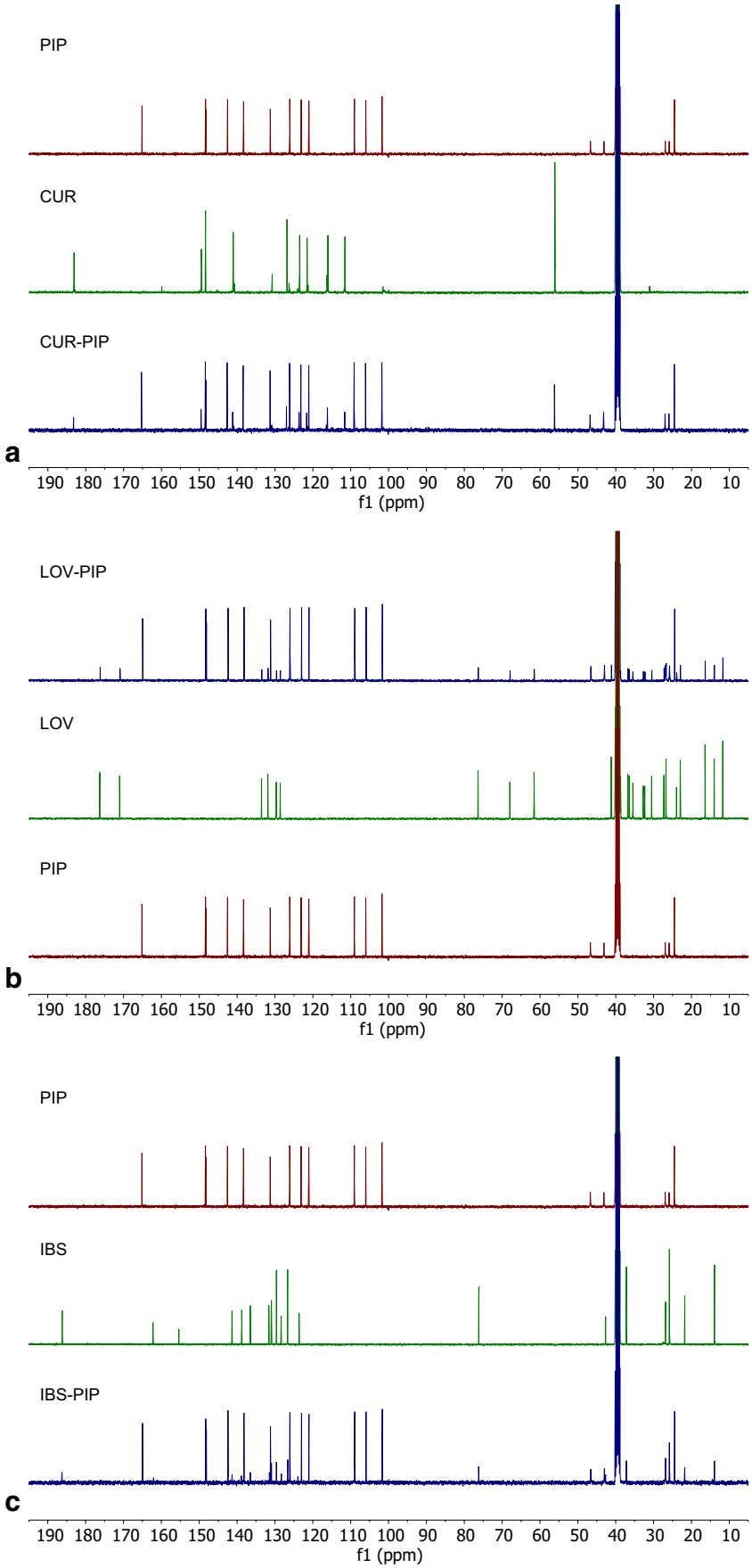

Fig. 12 Solution-state ^{13}C NMR spectra of piperine (PIP) and **a** curcumin (CUR) and CUR-PIP, **b** lovastatin (LOV) and LOV-PIP, and **c** irbesartan (IBS) and IBS-PIP

Table IV ^{13}C-NMR Chemical Shift Comparison Between EM and Their Constituents

	Pure compound[a]		$EM_{CUR-PIP}$		$EM_{LOV-PIP}$		$EM_{IBS-PIP}$	
	#C	δ (ppm)	δ (ppm)	Δ δ (ppm)	δ (ppm)	Δ δ (ppm)	δ (ppm)	Δ δ (ppm)
PIP signals	1	165.01	165.23	−0.22	165.11	−0.10	165.23	−0.22
	2	121.11	121.27	−0.16	121.09	0.02	121.27	−0.16
	3	142.41	142.65	−0.24	142.49	−0.08	142.29	0.12
	4	126.16	126.05	0.11	126.10	0.06	126.08	0.08
	5	138.40	138.50	−0.10	138.36	0.04	138.06	0.34
	1', 3'	148.06	148.22	−0.16	148.33	−0.27	148.44	−0.38
	2'	101.56	101.79	−0.23	101.70	−0.14	101.92	−0.36
	4'	106.14	106.06	0.08	106.03	0.11	106.06	0.08
	5'	131.34	131.21	0.13	131.19	0.15	131.19	0.15
	6'	123.14	123.15	−0.01	122.96	0.18	123.03	0.11
	7'	109.00	109.07	−0.07	108.99	0.01	108.94	0.06
	2"	43.25	43.27	−0.02	43.04	0.21	43.04	0.21
	3"	25.75	25.58	0.17	25.85	−0.10	25.86	−0.11
	4"	24.26	24.98	−0.72	24.43	−0.17	24.23	0.03
	5"	26.98	26.94	0.04	26.92	0.06	27.16	−0.18
	6"	46.68	46.74	−0.06	46.62	0.06	46.62	0.06
CUR signals	-OMe	56.15	56.15	0.00				
	1	101.48	101.59	−0.11				
	2, 2'	183.47	183.15	0.32				
	3, 3'	121.49	120.99	0.50				
	4, 4'	141.29	141.07	0.22				
	5, 5'	127.06	126.9	0.16				
	6, 6'	111.63	111.4	0.23				
	7, 7'	148.44	148.22	0.22				
	8, 8'	149.35	149.35	0.00				
	9, 9'	116.22	116.05	0.17				
	10, 10'	123.14	123.54	−0.40				
LOV signals	1	67.90			67.8	0.10		
	2	32.32			32.27	0.05		
	3	27.23			27.23	0.00		
	4	128.60			128.02	0.58		
	4a	131.86			131.87	−0.01		
	5	129.50			129.10	0.40		
	6	133.45			133.43	0.02		
	7	30.53			30.55	−0.02		
	8	36.46			36.40	0.06		
	8a	36.79			36.76	0.03		
	9	22.93			22.98	−0.05		
	10	14.00			14.02	−0.02		
	1'	171.15			171.10	0.05		
	2'	38.73			38.70	0.03		
	3'	61.58			61.71	−0.13		
	4'	35.47			35.55	−0.08		
	5'	76.28			76.31	−0.03		
	6'	32.67			32.72	−0.05		
	7'	24.00			23.95	0.05		
	1"	176.26			176.34	−0.08		
	2"	41.21			41.23	−0.02		
	3"	26.71			26.65	0.06		
	4"	11.76			11.82	−0.06		
	5"	16.40			16.46	−0.06		

Table IV (continued)

	Pure compound[a]		$EM_{CUR-PIP}$		$EM_{LOV-PIP}$		$EM_{IBS-PIP}$	
	#C	δ (ppm)	δ (ppm)	Δ δ (ppm)	δ (ppm)	Δ δ (ppm)	δ (ppm)	Δ δ (ppm)
IBS signals	2	162.24					162.09	0.15
	4	76.25					76.17	0.08
	5	186.18					186.38	−0.20
	7, 8	25.95					25.86	0.09
	6, 9	37.25					37.11	0.14
	10	42.67					42.82	−0.15
	11	136.51					136.49	0.02
	12, 16	126.51					126.62	−0.11
	13, 15	129.67					129.54	0.13
	14	138.92					138.92	0.00
	17	141.35					141.37	−0.02
	18	123.58					123.99	−0.41
	19, 22	130.94					130.93	0.01
	20	128.38					128.35	0.03
	21	131.69					131.68	0.01
	23	155.50					155.18	0.32
	28	26.89					27.16	−0.27
	29	26.79					26.76	0.03
	30	21.82					22.09	−0.27
	31	14.03					13.84	0.19

[a]Signals correspond to pure PIP and pure drugs CUR, LOV, and IBS measured in independent experiments

CUR, LOV and IBS in aqueous solution. NMR results suggested two main mechanisms for EM's interaction including hydrogen bonding and hydrophobic interaction corresponding to protons or carbons near electronegative sites on each of the four molecules involved. Therefore, indicating the presence of polar intermolecular interactions among them in solution. The coexistence of hydrophobic and electrostatic interaction, which was suggested from increase of the solubility confirmed by solution-state NMR study.

CONCLUSION

PIP was able to form multicomponent organic materials with CUR, LOV, and IBS, specifically EM confirmed by DSC, PXRD, and FT-IR analyses. The eutectic composition was calculated by both binary phase's and Tammann's diagrams. The preparation of these EM leads to enhanced solubility and dissolution rate of CUR, LOV, and IBS, through increases in wettability observed in the angle contact measurements specially for CUR-PIP and LOV-PIP meanwhile for IBS-PIP solubility improvement was not proportional with wettability increasing. No significant intermolecular interactions in solution between drugs and PIP in the three EM were observed through solution-state NMR. Therefore, this study presents a promising and practical approach to improve the solubility and dissolution rate for enhanced bioavailability of these drugs.

Supplementary Information The online version contains supplementary material available at https://doi.org/10.1208/s12249-022-02270-4.

Acknowledgements Authors thank to Dr Oscar Rojas Carrillo and M. Sc. Marianelly Esquivel Alfaro for the support given in the use of the dissolution test system.

Author Contribution Conceptualization A.M.A.-S.; methodology, K.W., A.M.A.-S., F.V., M.Q. and M.N.-H.; formal analysis, K.W., F.V., M.Q.; investigation, K.W., A.M.A.-S., F.V., M.N.-H.; resources, T.G-G., J.R.V.-B., M.N.-H., A.M.A.-S.; data curation, K.W., A.M.A.-S., M.Q., F.V., M.N.-H.; writing—original draft preparation, K.W., A.M.A.-S., M.Q., F.V.; writing—review and editing, T.G-G., J.R.V.-B., M.N.-H., A.M.A.-S.; supervision, T.G-G., A.M.A.-S., J.R.V.-B., M.N.-H.; project administration, T.G-G., A.M.A.-S., M.N.-H.; funding acquisition, T.G-G., J.R.V.-B., M.N.-H. and A.M.A.S. All authors have read and agreed to the published version of the manuscript.

Funding This contribution was partially funded by a grant from FEES-CONARE (Ref 115B9670). The financial support from the University of Costa Rica (UCR, Ref 115B6163), the Costa Rica Institute of Technology (TEC), the National Laboratory of Nanotechnology (LANOTEC CENAT), and the Technical University of Costa Rica (UTN).

Declarations

Conflict of interest The authors declare no competing interests.

References

1. World-Health-Organization. Health statistics and information systems Disease burden and mortality estimates [Internet]. 2020 [cited 2021 Feb 1]. Available from: https://www.who.int/data/gho/data/themes/mortality-and-global-health-estimates
2. Castillo-Rivas J. Atención de la enfermedades cardiovasculares en la Caja Costarricense de Seguro Social:: 1998 -2005. Scielo. 2006.
3. Luengo-Fernandez R. Cost of cardiovascular diseases in the United Kingdom. Heart. 2006;92:1384–9.
4. Pérez-Gonzales K. CCSS invierte ¢245.350 millones en atención de pacientes con enfermedades cardiovasculares. 2017. San José, Costa Rica; 2017;
5. Cooper R, Cutler J, Desvigne-Nickens P, Fortmann SP, Friedman L, Havlik R, et al. Trends and disparities in coronary heart disease, stroke, and other cardiovascular diseases in the United States. Circulation. 2000;102:3137–47.
6. Andreassen M, Raymond I, Kistorp C, Hildebrandt P, Faber J, Kristensen LØ. IGF1 as predictor of all cause mortality and cardiovascular disease in an elderly population. Eur J Endocrinol. 2009;160:25–31.
7. Li H, Sureda A, Devkota HP, Pittalà V, Barreca D, Silva AS, *et al*. Curcumin, the golden spice in treating cardiovascular diseases. Biotechnol Adv. 2020;38:107343.
8. Zolkiflee NF, Affandi MMRMM, Majeed ABA. Thermodynamics and solute-solvent interactions of lovastatin in an aqueous arginine solution. Eur J Pharm Sci. 2020;141:105111.
9. Leve S, Banga H, Shankar P, Dixit R. An experimental study of a novel combination of a herbal drug with an allopathic drug to evaluate the antihyperglycemic effect of irbesartan plus curcumin and comparison with glibenclamide. Int J Basic Clin Pharmacol. 2013;2:182.
10. Campbell MS, Fleenor BS. The emerging role of curcumin for improving vascular dysfunction: a review. Crit Rev Food Sci Nutr. 2018;58:2790–9.
11. Salehi B, Del Prado-Audelo ML, Cortés H, Leyva-Gómez G, Stojanović-Radić Z, Singh YD, et al. Therapeutic applications of curcumin nanomedicine formulations in cardiovascular diseases. J Clin Med. 2020;9:746.
12. Song Y, Chen J, Sun M, Gong C, Shen Y, Song Y, *et al*. A simple electrochemical biosensor based on AuNPs/MPS/Au electrode sensing layer for monitoring carbamate pesticides in real samples. J Hazard Mater. 2016;
13. Bi X, Yuan Z, Qu B, Zhou H, Liu Z, Xie Y. Piperine enhances the bioavailability of silybin via inhibition of efflux transporters BCRP and MRP2. Phytomedicine. 2019;54:98–108.
14. Zhang B, Yang J, Qin Z, Li S, Xu J, Yao Z, *et al*. Mechanism of the efflux transport of demethoxycurcumin-O-glucuronides in HeLa cells stably transfected with UDP-glucuronosyltransferase 1A1. Hsieh Y-H, editor. PLoS One. 2019;14:e0217695.
15. Phansalkar PS, Zhang Z, Verenich S, Gerk PM. Pharmacokinetics and bioavailability enhancement of natural products. Nat Prod Cancer Chemoprevention. Cham: Springer International Publishing; 2020. p. 109–41.
16. Wang L, Sun R, Zhang Q, Luo Q, Zeng S, Li X, et al. An update on polyphenol disposition via coupled metabolic pathways. Expert Opin Drug Metab Toxicol. 2019;15:151–65.
17. Lipinski CA. Drug-like properties and the causes of poor solubility and poor permeability. J Pharmacol Toxicol Methods. 2000;44:235–49.
18. Araya-Sibaja AM, Fandaruff C, Wilhelm K, Vega-Baudrit JR, Guillén-Girón T, Navarro-Hoyos M. Crystal engineering to design of solids: from single to multicomponent organic materials. Mini Rev Org Chem [Internet]. 2020;17:518–38. Available from: http://www.eurekaselect.com/171925/article
19. Vippagunta SR, Wang Z, Hornung S, Krill SL. Factors affecting the formation of eutectic solid dispersions and their dissolution behavior. J Pharm Sci [Internet]. 2007;96:294–304. Available from: http://linkinghub.elsevier.com/retrieve/pii/S0022354916321943
20. Kumar S, Nanda A. Approaches to design of pharmaceutical cocrystals: a review. Mol Cryst Liq Cryst. 2018;667:54–77.
21. Rathi N, Paradkar A, Gaikar VG. Polymorphs of curcumin and its cocrystals with cinnamic acid. J Pharm Sci. 2019;108:2505–16.
22. Sathisaran I, Dalvi SV. Crystal engineering of curcumin with salicylic acid and hydroxyquinol as coformers. Cryst Growth Des [Internet]. 2017;17:3974–88. Available from: http://pubs.acs.org/doi/https://doi.org/10.1021/acs.cgd.7b00599
23. Suresh K, Nangia A. Curcumin: pharmaceutical solids as a platform to improve solubility and bioavailability. CrystEngComm [Internet]. 2018; Available from: http://xlink.rsc.org/?DOI=C8CE00469B
24. Wang R, Han J, Jiang A, Huang R, Fu T, Wang L, *et al*. Involvement of metabolism-permeability in enhancing the oral bioavailability of curcumin in excipient-free solid dispersions co-formed with piperine. Int J Pharm [Internet]. 2019;561:9–18. Available from: https://linkinghub.elsevier.com/retrieve/pii/S0378517319301504
25. Singh J, Dubey RK, Atal CK. Piperine-mediated inhibition of glucuronidation activity in isolated epithelial cells of the guinea-pig small intestine: evidence that piperine lowers the endogeneous UDP-glucuronic acid content. J Pharmacol Exp Ther. 1986;236.
26. FDA. CFR - Code of Federal Regulations Title 21-Food aditives permitted for direct addition to food for human consumptions.
27. Chadha K, Karan M, Chadha R, Bhalla Y, Vasisht K. Is failure of cocrystallization actually a failure? Eutectic formation in cocrystal screening of hesperetin. J Pharm Sci [Internet]. 2017;106:2026–36. Available from: https://linkinghub.elsevier.com/retrieve/pii/S0022354917302745
28. Araya-Sibaja A, Vega-Baudrit J, Guillén-Girón T, Navarro-Hoyos M, Cuffini S. Drug solubility enhancement through the preparation of multicomponent organic materials: eutectics of lovastatin with carboxylic acids. Pharmaceutics [Internet]. 2019;11:112. Available from: https://www.mdpi.com/1999-4923/11/3/112
29. Rycerz L. Practical remarks concerning phase diagrams determination on the basis of differential scanning calorimetry measurements. J Therm Anal Calorim [Internet]. 2013;113:231–8. Available from: http://link.springer.com/https://doi.org/10.1007/s10973-013-3097-0
30. Höhne GWH, Hemminger WF, Flammersheim H-J. Differential scanning calorimetry [Internet]. Berlin, Heidelberg: Springer Berlin Heidelberg; 2003. Available from: http://link.springer.com/https://doi.org/10.1007/978-3-662-06710-9
31. Gaisford S, Kett V, Haines P, editors. Principles of thermal analysis and calorimetry. The Royal Society of Chemistry; 2016.

32. Boettinger WJ, Kattner UR, Moon K-W, Perepezko JH. Methods for phase diagram determination [Internet]. Zhao J-C, editor. Elsevier; 2007. Available from: https://linkinghub.elsevier.com/retrieve/pii/B9780080446295X50009
33. FDA. Guidance for industry dissolution testing of immediate solid oral dosage form [Internet]. 1997. Available from: http://www.fda.gov/downloads/Drugs/.../Guidances/ucm070246.pdf
34. Swanepoel E, Liebenberg W, de Villiers MM. Quality evaluation of generic drugs by dissolution test: changing the USP dissolution medium to distinguish between active and non-active mebendazole polymorphs. Eur J Pharm Biopharm [Internet]. 2003;55:345–9. Available from: http://linkinghub.elsevier.com/retrieve/pii/S0939641103000043
35. Honorato SB, Farfan S, Viana A, Filho JM, Camar??o GC, Fechine F V., *et al*. Polymorphism evaluation in generic tablets containing mebendazole by dissolution tests. J Braz Chem Soc. 2012;23:220–7.
36. Moorthi C, Senthil Kumar C, Mohan S, Krishnan K, Kathiresan K. Application of validated RP–HPLC–PDA method for the simultaneous estimation of curcumin and piperine in Eudragit E 100 nanoparticles. J Pharm Res [Internet]. 2013;7:224–9. Available from: https://linkinghub.elsevier.com/retrieve/pii/S097469431300114X
37. PubChem. Lovastatin Water Solubility [Internet]. [cited 2021 Feb 1]. Available from: https://pubchem.ncbi.nlm.nih.gov/compound/Lovastatin#section=Solubility&fullscreen=true
38. PubChem. Irbesartan Water Solubility [Internet]. [cited 2021 Aug 21]. Available from: https://pubchem.ncbi.nlm.nih.gov/compound/Irbesartan#section=Solubility&fullscreen=true
39. PubChem. Curcumin Water Solubility [Internet]. [cited 2021 Jan 10]. Available from: https://pubchem.ncbi.nlm.nih.gov/compound/Curcumin#section=Solubility&fullscreen=true
40. Martins GS. Differential Scanning Thermal Analysis of Shape-Memory Polymers, Polymer Blends and Composites. 2020. p. 153–66.
41. Chaturvedi K, Shah HS, Nahar K, Dave R, Morris KR. Contribution of crystal lattice energy on the dissolution behavior of eutectic solid dispersions. ACS Omega. 2020;5:9690–701.
42. Lin B, Liu Y, Wang M, Wang Y, Du S, Gong J, et al. Intermolecular interactions and solubility behavior of multicomponent crystal forms of orotic acid: prediction and experiments. Cryst Growth Des. 2021;21:1473–81.
43. Moore MD, Wildfong PLD. Aqueous solubility enhancement through engineering of binary solid composites: pharmaceutical applications. J Pharm Innov. 2009;4:36–49.
44. Jackson KA, Hunt JD. Lamellar and rod eutectic growth. Dyn Curved Front. Elsevier; 1988. p. 363–76.
45. Jain H, Khomane KS, Bansal AK. Implication of microstructure on the mechanical behaviour of an aspirin–paracetamol eutectic mixture. CrystEngComm [Internet]. 2014;16:8471–8. Available from: http://xlink.rsc.org/?DOI=C4CE00878B
46. Fiandaca M, Dalwadi G, Wigent R, Gupta P. Ionic liquid formation with deep eutectic forces at an atypical ratio (2:1) of naproxen to lidocaine in the solid-state, thermal characterization and FTIR investigation. Int J Pharm. 2020;575:118946.
47. Meira RZC, Biscaia IFB, Nogueira C, Murakami FS, Bernardi LS, Oliveira PR. Solid-state characterization and compatibility studies of penciclovir, lysine hydrochloride, and pharmaceutical excipients. Materials (Basel). 2019;12:3154.
48. Gandolfo FG, Bot A, Flöter E. Phase diagram of mixtures of stearic acid and stearyl alcohol. Thermochim Acta. 2003;404:9–17.
49. Patel RD, Raval MK, Sheth NR. Formation of diacerein – fumaric acid eutectic as a multi-component system for the functionality enhancement. J Drug Deliv Sci Technol. 2020;58:101562.
50. Hyun S-M, Lee BJ, Abuzar SM, Lee S, Joo Y, Hong S-H, *et al*. Preparation, characterization, and evaluation of celecoxib eutectic mixtures with adipic acid/saccharin for improvement of wettability and dissolution rate. Int J Pharm [Internet]. 2019;554:61–71. Available from: https://linkinghub.elsevier.com/retrieve/pii/S0378517318307841
51. Leitner J, Jurik S. DSC study and thermodynamic modelling of the system paracetamol–o-acetylsalicylic acid. J Therm Anal Calorim [Internet]. 2017;130:1735–40. Available from: http://link.springer.com/https://doi.org/10.1007/s10973-017-6404-3
52. Dichi E, Sghaier M, Guiblin N. Reinvestigation of the paracetamol–caffeine, aspirin–caffeine, and paracetamol–aspirin phase equilibria diagrams. J Therm Anal Calorim [Internet]. 2018;131:2141–55. Available from: http://link.springer.com/https://doi.org/10.1007/s10973-017-6855-6
53. Rathod MK, Banerjee J. Thermal stability of phase change materials used in latent heat energy storage systems: A review. Renew Sustain Energy Rev. 2013;18:246–58.
54. Das SS, Singh NP, Agrawal T, Gupta P, Tiwari SN, Singh NB. Studies of solidification behavior and molecular interaction in benzoic acid–o-chloro benzoic acid eutectic system. Mol Cryst Liq Cryst. 2009;501:107–24.
55. Li W, Shi P, Jia L, Zhao Y, Sun B, Zhang M, *et al*. Eutectics and salt of dapsone with hydroxybenzoic acids: binary phase diagrams, characterization and evaluation. J Pharm Sci. 2020;
56. Larkin P. Environmental dependence of vibrational spectra. Infrared Raman Spectrosc [Internet]. Elsevier; 2011. p. 55–62. Available from: https://linkinghub.elsevier.com/retrieve/pii/B9780123869845100047
57. Taylor R, Wood PA. A million crystal structures: the whole is greater than the sum of its parts. Chem Rev [Internet]. 2019;119:9427–77. Available from: https://pubs.acs.org/doi/https://doi.org/10.1021/acs.chemrev.9b00155
58. Desiraju GR. Crystal engineering: from molecule to crystal. J Am Chem Soc [Internet]. 2013 [cited 2014 May 28];135:9952–67. Available from: http://www.ncbi.nlm.nih.gov/pubmed/23750552
59. Desiraju GR. Crystal engineering: a holistic view. Angew Chem Int Ed Engl [Internet]. 2007 [cited 2014 May 19];46:8342–56. Available from: http://www.ncbi.nlm.nih.gov/pubmed/17902079
60. Dahiya S, Rani R, Dhingra D, Kumar S, Dilbaghi N. Conjugation of epigallocatechin gallate and piperine into a zein nanocarrier: implication on antioxidant and anticancer potential. Adv Nat Sci Nanosci Nanotechnol. 2018;9:035011.
61. Zaini E, Afriyani A, Fitriani L, Ismed F, Horikawa A, Uekusa H. Improved solubility and dissolution rates in novel multicomponent crystals of piperine with succinic acid. Sci Pharm. 2020;88:21.
62. Górniak A, Gajda M, Pluta J, Czapor-Irzabek H, Karolewicz B. Thermal, spectroscopic and dissolution studies of lovastatin solid dispersions with acetylsalicylic acid. J Therm Anal Calorim. 2016;
63. Cherukuvada S, Nangia A. Eutectics as improved pharmaceutical materials: design, properties and characterization. Chem Commun [Internet]. 2014;50:906–23. Available from: http://xlink.rsc.org/?DOI=C3CC47521B
64. Park H, Seo HJ, Ha E-S, Hong S, Kim J-S, Kim M-S, *et al*. Preparation and characterization of glimepiride eutectic mixture with l-arginine for improvement of dissolution rate. Int J Pharm [Internet]. 2020;581:119288. Available from: https://linkinghub.elsevier.com/retrieve/pii/S0378517320302726
65. Araya-Sibaja AM, Maduro Campos CE, Fandaruff C, Vega-Baudrit JR, Guillén-Girón T, Hoyos MN, *et al*. Irbesartan desmotropes: Solid-state characterization, thermodynamic study and dissolution properties. J Pharm Anal [Internet]. 2019; Available

from: https://linkinghub.elsevier.com/retrieve/pii/S2095177919300814
66. Pandey KU, Dalvi SV. Understanding stability relationships among three curcumin polymorphs. Adv Powder Technol [Internet]. 2019;30:266–76. Available from: https://linkinghub.elsevier.com/retrieve/pii/S0921883118308392
67. Patel M, Tekade A, Gattani S, Surana S. Solubility enhancement of lovastatin by modified locust bean gum using solid dispersion techniques. AAPS PharmSciTech [Internet]. 2008 [cited 2014 Jun 4];9:1262–9. Available from: http://www.pubmedcentral.nih.gov/articlerender.fcgi?artid=2628263&tool=pmcentrez&rendertype=abstract
68. Yoshida MI, Oliveira MA, Gomes ECL, Mussel WN, Castro W V., Soares CD V. Thermal characterization of lovastatin in pharmaceutical formulations. J Therm Anal Calorim [Internet]. 2011;106:657–64. Available from: http://link.springer.com/https://doi.org/10.1007/s10973-011-1510-0
69. Nicolaides E, Galia E, Efthymiopoulos C, Dressman JB, Reppas C. Forecasting the in vivo performance of four low solubility drugs from their in vitro dissolution data. Pharm. Res. 1999. p. 1876–82.
70. Zaborenko N, Shi Z, Corredor CC, Smith-Goettler BM, Zhang L, Hermans A, *et al*. First-principles and empirical approaches to predicting in vitro dissolution for pharmaceutical formulation and process development and for product release testing. AAPS J [Internet]. 2019;21:32. Available from: http://link.springer.com/https://doi.org/10.1208/s12248-019-0297-y
71. Dressman JB, Reppas C. In vitro–in vivo correlations for lipophilic, poorly water-soluble drugs. Eur J Pharm Sci [Internet]. 2000;11:S73–80. Available from: https://linkinghub.elsevier.com/retrieve/pii/S0928098700001810
72. Gómez SM, Martínez JA, Martínez F. Validación de un método analítico empleando cromatografía líquida de alta eficiencia para la determinación de ibuprofeno en medios biorrelevantes. Quim Nova. 2010;33:1794–9.
73. Bhattachar SN, Risley DS, Werawatganone P, Aburub A. Weak bases and formation of a less soluble lauryl sulfate salt/complex in sodium lauryl sulfate (SLS) containing media. Int J Pharm. 2011;412:95–8.
74. Huang Z, Parikh S, Fish WP. Interactions between a poorly soluble cationic drug and sodium dodecyl sulfate in dissolution medium and their impact on in vitro dissolution behavior. Int J Pharm. 2018;535:350–9.
75. Guo Y, Wang C, Dun J, Du L, Hawley M, Sun CC. Mechanism for the reduced dissolution of ritonavir tablets by sodium lauryl sulfate. J Pharm Sci. 2019;108:516–24.
76. Fandaruff C, Rauber GS, Araya-Sibaja AM, Pereira RN, de Campos CEM, Rocha HVA, *et al*. Polymorphism of anti-HIV drug efavirenz: investigations on thermodynamic and dissolution properties. Cryst Growth Des [Internet]. 2014 [cited 2014 Nov 7];14:4968–75. Available from: http://pubs.acs.org/doi/abs/https://doi.org/10.1021/cg500509c
77. Fandaruff C, Segatto Silva MA, Galindo Bedor DC, de Santana DP, Rocha HVA, Rebuffi L, *et al*. Correlation between microstructure and bioequivalence in anti-HIV drug efavirenz. Eur J Pharm Biopharm [Internet]. 2015;91:52–8. Available from: http://linkinghub.elsevier.com/retrieve/pii/S0939641115000363
78. Madhuri G, Nagaraju R, Killari KN. Enhancement of the physicochemical properties of poorly soluble lovastatin by co-crystallization techniques - in vivo studies. Indian J Pharm Sci [Internet]. 2020;82. Available from: https://www.ijpsonline.com/articles/enhancement-of-the-physicochemical-properties-of-poorly-soluble-lovastatin-by-cocrystallization-techniques--in-vivo-studies-3865.html
79. Rachmawati H, Edityaningrum CA, Mauludin R. Molecular inclusion complex of curcumin–β-cyclodextrin nanoparticle to enhance curcumin skin permeability from hydrophilic matrix gel. AAPS PharmSciTech [Internet]. 2013;14:1303–12. Available from: http://link.springer.com/https://doi.org/10.1208/s12249-013-0023-5
80. Zhang Z, Le Y, Wang J, Zhao H, Chen J. Irbesartan drug formulated as nanocomposite particles for the enhancement of the dissolution rate. Particuology [Internet]. 2012 [cited 2014 May 14];10:462–7. Available from: http://linkinghub.elsevier.com/retrieve/pii/S1674200112000296
81. Suryadevara V, Lankapalli S, Sunkara S, Sakhamuri V, Danda H. Dissolution rate enhancement of irbesartan and development of fast-dissolving tablets. Egypt Pharm J [Internet]. 2016;15:150. Available from: http://www.epj.eg.net/text.asp?2016/15/3/150/197583
82. Traxler F, Schinnerl J, Brecker L. Spectroscopic studies on the molecular interactions of curcumin and piperine. Monatshefte für Chemie - Chem Mon [Internet]. 2020;151:325–30. Available from: http://link.springer.com/https://doi.org/10.1007/s00706-020-02563-z
83. Kumar V, Mintoo MJ, Mondhe DM, Bharate SB, Vishwakarma RA, Bharate SS. Binary and ternary solid dispersions of an anticancer preclinical lead, IIIM-290: In vitro and in vivo studies. Int J Pharm [Internet]. 2019;570:118683. Available from: https://linkinghub.elsevier.com/retrieve/pii/S0378517319307288